Tyrosinase-induced neuromelanin accumulation triggers rapid dysregulation and degeneration of the mouse locus coeruleus

Alexa F. Iannitelli[1*], Leslie Hassenein[1*], Bernard Mulvey[2,3,4], Harris E. Blankenship[5], L. Cameron Liles[1], Amanda L. Sharpe[6], Jean-Francoise Pare[7,8], Arielle Segal[1], Steven A. Sloan[1], Keri Martinowich[3,4], Katharine E. McCann[1], Joseph D. Dougherty[2], Yoland Smith[7,8], Michael J. Beckstead[5], David Weinshenker[1#]

[*]Equal contributions

[1]Department of Human Genetics, Emory University School of Medicine, Atlanta, GA 30322, USA

[2]Department of Psychiatry, Intellectual and Developmental Disabilities Research Center, Washington University School of Medicine, St. Louis, MO 63110, USA

[3]Lieber Institute for Brain Development, Johns Hopkins Medical Campus, Baltimore, MD, 21205, USA.

[4]Department of Psychiatry and Behavioral Sciences, Johns Hopkins School of Medicine, Baltimore, MD, 21205, USA.[2]Department of Genetics, Washington University School of Medicine, St. Louis, MO 63110, USA

[5]Aging & Metabolism Research Program, Oklahoma Medical Research Foundation, Oklahoma City, OK 73104

[6]Department of Pharmaceutical Sciences, University of Oklahoma Health Sciences Center, Oklahoma City, 73117

[7]Department of Neurology, Emory University School of Medicine, Atlanta, GA 30322, USA

[8]Emory National Primate Research Center, Emory University, Atlanta, GA 30329, USA

[#]Address correspondence to:

David Weinshenker, PhD

Department of Human Genetics

Emory University School of Medicine

615 Michael St., Whitehead 301

Phone: (404) 727-3106

Email: dweinsh@emory.edu

Abstract

The locus coeruleus (LC), the major source of norepinephrine (NE) in the brain, is an early site of pathology in both Alzheimer's disease (AD) and Parkinson's disease (PD), and it undergoes catastrophic degeneration later in both disorders. Dysregulation of the LC is thought to contribute to prodromal symptoms of AD and PD such as anxiety and sleep disturbances, while frank LC-NE loss promotes cognitive decline. However, the mechanisms responsible for its selective vulnerability are unknown. The LC is among the only structures in the brain that produces appreciable amounts of neuromelanin (NM), a dark cytoplasmic pigment. It has been proposed that NM initially plays a protective role by sequestering toxic catecholamine metabolites and heavy metals, but may become harmful during aging as it overwhelms cellular machinery and is released during neurodegeneration. Rodents do not naturally produce NM, limiting the study of causal relationships between NM and LC pathology. Adapting a viral-mediated approach for expression of human tyrosinase, the enzyme responsible for peripheral melanin production, we successfully promoted pigmentation in mouse LC neurons that recapitulates key ultrastructural features of endogenous NM found in primates. Pigment expression results in LC neuron hyperactivity, reduced tissue NE levels, transcriptional changes, and novelty-induced anxiety phenotypes as early as 1-week post-injection. By 6-10 weeks, NM accumulation is associated with severe LC neuron neurodegeneration and microglial engulfment of the pigment granules, while the anxiety-like behavior is abated. These phenotypes are reminiscent of LC dysfunction and cell death in AD and PD, validating this model for studying the consequences of pigment accumulation in the LC as it relates to neurodegenerative disease.

Introduction

The neurodegenerative diseases Alzheimer's disease (AD) and Parkinson's disease (PD) are among the most common causes of dementia and movement disorders, respectively. The noradrenergic locus coeruleus (LC), the major source of central norepinephrine (NE) is one of the earliest brain regions to accumulate tau pathology in AD and α-synuclein pathology in PD (Braak et al., 2001; Del Tredici et al., 2002; Braak and Del Tredici, 2011a, b; Braak et al., 2011; Pletnikova et al., 2018; Gilvesy et al., 2022; Bueicheku et al., 2024), and it undergoes catastrophic degeneration later in both diseases (Mann et al., 1980; Bondareff et al., 1982; Iversen et al., 1983; Mann and Yates, 1983b; German et al., 1992; Zarow et al., 2003; Theofilas et al., 2017). Both clinical and animal model research has identified early LC-NE dysfunction as a trigger for prodromal symptoms in AD and PD typified by sleep abnormalities and neuropsychiatric symptoms such as anxiety, depression, and apathy (Remy et al., 2005; Prediger et al., 2012; Ehrenberg et al., 2017; Ehrenberg et al., 2018; Sommerauer et al., 2018; Weinshenker, 2018; Butkovich et al., 2020; Gilvesy et al., 2022; Kelberman et al., 2022; Ye et al., 2022; Iannitelli et al., 2023b; Falgas et al., 2024), while subsequent frank LC degeneration predicts and exacerbates cognitive decline (Zweig et al., 1993; Heneka et al., 2006; Vazey and Aston-Jones, 2012; Rorabaugh et al., 2017; Chalermpalanupap et al., 2018; Weinshenker, 2018; Ghosh et al., 2019; Li et al., 2019; Jacobs et al., 2021; Prokopiou et al., 2022; Ye et al., 2022; Bueicheku et al., 2024). experimental manipulations of the LC faithfully recapitulate non-motor symptoms in animal models (Mavridis et al., 1991; Srinivasan and Schmidt, 2003; Song et al., 2019; Iannitelli et al., 2023b).

The specific factors that make LC neurons vulnerable to pathology, dysfunction, and death in AD and PD are not fully understood, although several potential contributors have been identified

(Weinshenker, 2018; Kang et al., 2020; Matchett et al., 2021; Kang et al., 2022; Iannitelli et al., 2023a; Iannitelli and Weinshenker, 2023). The LC projects to virtually every other region of the brain, resulting in long, highly branched, unmyelinated axons. LC neurons also have intrinsic pacemaker activity, which leads to high levels of oxidative stress and risk for mitochondrial dysfunction, factors which are well-studied in relation to neurodegenerative disease. Additionally, these noradrenergic neurons harbor toxic NE metabolites such as 3,4-dihydroxyphenylglycoaldehyde (DOPEGAL) that can promote pathology. Perhaps the most defining characteristic of these neurons, though, is their unique expression of a dark, cytoplasmic pigment called neuromelanin (NM).

NM is found exclusively in catecholaminergic cells of the LC and substantia nigra (SN), which is also vulnerable in PD (Zecca et al., 2004; Zecca et al., 2008b). NM is a byproduct of catecholamine synthesis and metabolism, and studies suggest that the formation of NM granules likely results from an overabundance of catecholamines that cannot be sequestered into vesicles quickly enough in active neurons (Sulzer et al., 2000). In addition to catecholamine metabolites, these granules contain melanins (Bush et al., 2006), lipid droplets, protein aggregates (Sulzer et al., 2008), and heavy metals, most notably iron and copper (Zecca et al., 2008b). Thus, it has been proposed that the primary function of NM is to bind and sequester these harmful compounds in the cytoplasm so that they do not harm the neurons (Zecca et al., 2003). However, because LC-NE neurons do not possess the machinery required to break down these granules, NM accumulates over time, visibly darkening the pigmentation of these brain regions with age. Eventually, this buildup of NM within catecholamine neurons may exacerbate neurodegeneration in AD and PD either by interfering with and overwhelming cellular machinery and/or via release of previously bound toxins as it breaks down during cell death. Indeed, LC neurons containing the highest

amounts of NM are disproportionately lost during both normal aging and PD (Mann and Yates, 1983a), and increased iron (Sasaki et al., 2006), zinc (Dexter et al., 1992), and copper (Pall et al., 1987) are evident in brain and CSF samples from PD patients, suggesting dysregulation of heavy-metal homeostasis.

Despite the clear link between NM and neurodegeneration in PD, establishing a causal relationship has been difficult because NM is not produced endogenously in rodents (Barden and Levine, 1983), which comprise the majority of animal models for studying AD and PD. It is not clear why rats and mice do not produce NM. It could be due to fundamental neurobiological differences between primate and rodent catecholamine LC neurons, or it may reflect their comparatively short life span (~2 years). Indeed, one study did report trace amounts of NM in aged rats (DeMattei et al., 1986), and even humans do not express detectable amounts of NM in LC neurons until they are 3 years old (Mann and Yates, 1974). Thus, despite an ever-growing toolbox of mouse genetic technology that makes them ideal for investigating the molecular mechanisms of disease, *in vivo* studies on NM have been extremely limited. To date, only two rodent models of NM has been reported. The first study in rodents relied on purification and intracranial injection of human neuromelanin granules (Zecca et al., 2008a), but more recently, researchers were able to drive pigmentation in the SN of mice and rats through viral-mediated expression of human Tyrosinase (hTyr), the biosynthetic enzyme responsible for melanin production in the skin (Carballo-Carbajal et al., 2019). In this model, NM expression in the SN resulted in neurodegeneration and subsequent motor impairments similar to those seen in other mouse models of PD. We have adapted this strategy to promote NM accumulation in the mouse LC to gain insight into the molecular mechanisms of NM-mediated adaptations and neurotoxicity in a region of selective early vulnerability in AD and PD.

Materials and Methods

Animals. Adult male and female mice were used for all behavioral and immunohistochemical experiments. For immunohistochemistry, behavior, and HPLC, TH-Cre mice (B6.Cg-7630403G23RikTg(Th-cre)1Tmd/J, The Jackson Laboratory, # 008601) were used for the specific expression of Cre-dependent viral vectors in the LC. For translating ribosome affinity purification (TRAP) RNA-sequencing experiments, we crossed TH-Cre mice with transgenic *Slc6a2-eGFP/Rpl10a* mice (B6;FVB-Tg(*Slc6a2-eGFP/Rpl10a*)JD1538Htz/J, The Jackson Laboratory, #031151), which incorporate an EGFP/Rpl10a ribosomal fusion protein into a bacterial artificial chromosome under the *Slc6a2* (NE transporter; NET) promoter to allow for the isolation of polysomes and translating mRNAs specifically from noradrenergic neurons (Mulvey et al., 2018). Mice were group housed with sex- and age-matched conspecifics (maximum of 5 animals per cage) until one week prior to behavioral testing, and then individually housed for the subsequent week of experimentation until sacrifice. Animals were maintained on a 12:12 light:dark cycle (lights on at 0700), and food and water were available *ad libitum*, unless otherwise specified. All experiments were conducted at Emory University in accordance with the National Institutes of Health *Guideline for the Care and Use of Laboratory Animals* and approved by the Emory Institutional Animal Care and Use Committee.

Viral vectors. To express hTyr in the LC, we developed an AAV5-EF1a-DIO-hTyr construct with assistance from the Emory Custom Cloning and Viral Vector Cores. For some preliminary experiments (immunohistochemistry for viral confirmation and gliosis, stereology), all mice were injected with AAV5-DIO-hTyr, and TH-Cre+ animals were used as the experimental group while TH-Cre- littermates served as the controls. For the remaining experiments, only TH-Cre+ mice

were used, and mice were injected with either the AAV5-DIO-hTyr experimental virus or a comparable AAV5-DIO-EYFP control virus (Addgene, plasmid #27056).

Stereotaxic injections. Stereotaxic infusions were be performed as previously described (Tillage et al., 2020a), in a stereotaxic frame under 2.0% isoflurane anesthesia. Bilateral LC infusions were made at a volume of 0.5 µL/hemisphere using a 5 µL Hamilton glass syringe. The virus was infused at a rate of 0.15 µL/min, and the needle was allowed to remain in place for 5 min following the completion of each infusion. LC coordinates are AP: - 5.4mm, ML: +/- 1.2mm, and DV: -4.0mm relative to Bregma.

High Performance Liquid Chromatography (HPLC). Mice were anesthetized with isoflurane and euthanized by rapid decapitation. The pons, prefrontal cortex, and hippocampus were rapidly dissected on ice and flash-frozen in isopentane (2-Methylbutane) on dry ice. The samples were weighed and stored at -80°C until processing for HPLC by the Emory HPLC Bioanalytical Core. As previously described (Lustberg et al., 2022), tissue was thawed on ice and sonicated in 0.1 N perchloric acid (10 µl/mg tissue) for 12 s with 0.5 s pulses. Sonicated samples were centrifuged (16,100 rcf) for 30 min at 4 °C, and the supernatant was then centrifuged through 0.45 µm filters at 4000 rcf for 10 min at 4 °C. For HPLC, an ESA 5600A CoulArray detection system, equipped with an ESA Model 584 pump and an ESA 542 refrigerated autosampler was used. Separations were performed using an MD-150 × 3.2 mm C18, 3 µm column (Thermo Scientific) at 30 °C. The mobile phase consisted of 8% acetonitrile, 75 mM NaH2PO4, 1.7 mM 1-octanesulfonic acid sodium and 0.025% trimethylamine at pH 2.9. A 20 µL of sample was injected. The samples were eluted isocratically at 0.4 mL/min and detected using a 6210 electrochemical cell (ESA, Bedford,

MA) equipped with 5020 guard cell. Guard cell potential was set at 475 mV, while analytical cell potentials were −175, 100, 350 and 425 mV. The analytes were identified by the matching criteria of retention time measures to known standards (Sigma Chemical Co., St. Louis MO). Compounds were quantified by comparing peak areas to those of standards on the dominant sensor.

Immunohistochemistry. Mice were euthanized with an overdose of sodium pentobarbital (Fatal Plus, 150 mg/kg, i.p.; Med-Vet International, Mettawa, IL) and were transcardially perfused with cold 4% PFA in 0.01 M PBS for light microscopy and 4% PFA + 0.1% glutaraldehyde for electron microscopy. After extraction, brains were post-fixed overnight in 4% PFA at 4°C and then transferred to a 30% sucrose/PBS solution for 72 h at 4°C. Brains were embedded in OCT medium (Tissue-Tek) and sectioned by cryostat into 40-um-thick coronal sections at the level of the LC, anterior cingulate cortex (ACC), and hippocampus. Sections were blocked in 5% normal goat serum (NGS) in 0.01 M PBS/0.1% Triton-X permeabilization buffer and then incubated for 24 h at 4°C in NGS blocking buffer with primary antibodies listed in **Table 1**. Following washes in 0.01 M PBS, sections were incubated for 2 h in blocking buffer including secondary antibodies listed in **Table 1**. After washing, sections were mounted onto Superfrost Plus slides and cover-slipped with Fluoromount-G plus DAPI (Southern Biotech, Birmingham, AL).

Fluorescence Microscopy. For the catecholaminergic marker tyrosine hydroxylase (TH) and hTyr, immunofluorescent micrographs were acquired on a Leica DM6000B epifluorescent upright microscope at 20x magnification with uniform exposure parameters for each stain and region imaged. Brightfield images of pigment granules were also obtained on the Leica DM6000B upright microscope at 20x magnification. Following convention, these images are oriented with the dorsal

direction up and the ventral direction down. For astrocyte marker glial fibrillary acidic protein (GFAP) and LC terminal marker NE transporter (NET), listed in **Table 1**, immunofluorescent images were acquired as z-stack images (10 z-stacks; pitch: 0.1 µm) at 20x magnification and compressed on a Keyence BZ-X700 microscope system. One representative atlas-matched section was selected from each animal. Image processing for all images was conducted using the FIJI/ImageJ software.

Electron microscopy. Electron microscopy experiments were conducted by the laboratory of Dr. Yoland Smith at the Emory National Primate Research Center. All brains prepared for electron microscopy were cut in 60 mm-thick coronal sections with a vibrating microtome. Sections that included the locus coeruleus were rinsed in Phosphate buffer (PB; 0.1 M, pH 7.4) and then treated with 0.5% osmium tetroxide (OsO4) for 10 min (RT) and returned to PB. Sections were then dehydrated with increasing concentrations of ethanol; 1% uranyl acetate was added to the 70% ethanol solution to increase EM contrast (10 min incubation at RT in the dark). Sections were next placed in propylene oxide, followed by tissue embedding with an epoxy resin (Durcupan, Fluka) for at least 12 hr. Resin-embedded sections were then baked at 60°C for at least 48-hr until fully cured. Blocks containing the LC were removed before being cut into ultrathin 60 nm sections (Leica Ultracut T2). These ultrathin sections were mounted onto pioloform-coated grids and stained with lead citrate (5 min, RT) for added contrast. Grids were then examined with an electron microscope (EM; Jeol; Model 1011) coupled with a CCD camera (Gatan; Model 785) controlled with DigitalMicrograph software (Gatan; version 3.11.1).

For ultrastructual comparisons of hTyr-induced NM in mice and naturally produced NM in primates, three brainstem sections at the level of LC from a 16 year-old rhesus macaque were processed according to the same procedure and examined in the electron microscope.

Cell counts. Mice (n=3) were given a unilateral infusion of AAV5-DIO-hTyr virus targeting the LC. The contralateral LC was infused with AAV5-DIO-EYFP. One week later, animals were perfused as described above. Brains were sectioned at 40um on a cryostat, and sections were processed for immunohistochemistry to stain for TH and NISSL. Images were taken at 4x and 20x on a Keyence BZ-X800 microscope. A z-stack (2um pitch, 20 images total) was acquired for all 20x images and the full focus image was used for analysis. Brightfield images to capture NM expression were transformed into fluorescence images using HALO v3.6 Deconvolution (Indica Labs) and fused with fluorescence images of TH and NISSL. Cell counts were quantified using HALO v3.6 FISH-IF v2.1.4 software. Cells were defined using either NISSL or TH and then counted within the region of interest delineating the LC. LC borders were defined using TH and NM. Me5 cells, which fluoresce brightly in all channels and are much larger and rounder than LC cells, were excluded from the boundaries of analysis. Parameters used to define cells were set for each animal and used consistently across all sections for that animal.

Translating Ribosome Affinity Purification (TRAP). To obtain adequate quantities of RNA for sequencing, samples from two 6-8 month-old, same-sex and treatment TH-Cre+, *Slc6a2-eGFP*/*Rpl10a*+ mice were pooled to form a biological replicate by dissecting out the hindbrain posterior to the pontine/hypothalamic junction (cerebellum was discarded). Six biological replicates were collected per treatment group. Each replicate was homogenized and TRAP was performed as described (Mulvey et al., 2018; Iannitelli et al., 2022), resulting in LC-enriched

"TRAP" samples and whole-hindbrain "input" samples. RNA was extracted using Zymo RNA Clean & Concentrator-5 kit, and subsequently sent for polyA-enriched library preparation and Illumina sequencing by NovoGene to a minimum depth of 20 million fragments per sample. Forward and reverse sequencing files from each replicate were aligned to the mouse genome (mm10) using STAR alignment, and counts were obtained using FeatureCounts in R Bioconductor. Two samples from saline-treated mice were removed from analysis because the TRAP protocol failed to enrich *Slc6a2* above a 10-fold change, a quality control threshold observed in all other saline-treated samples. All subsequent analyses utilized R Bioconductor packages. Sequencing data are available on NCBI GEO (GSE226827).

To further characterize the gene expression changes, we performed analyses to compare gene expression patterns in our dataset with a repository of gene sets using Gene Set Enrichment Analysis (GSEA 4.2.3) (Mootha et al., 2003; Subramanian et al., 2005). Gene set permutation was used, as recommended by GSEA documentation for experiments with fewer than 7 samples per group. Other parameters were set to default settings using 1000 gene set permutations and signal to noise ranking metric. We downloaded KEGG Pathways from the Molecular Signatures Database, which has 186 gene sets. After filtering for the recommended minimum (15) and maximum (500) gene set size, the remaining 145 gene sets were compared to the expression data from our dataset to calculate the GSEA enrichment score and to compute significant enrichment.

Electrophysiology. Mice were deeply anesthetized with isoflurane and decapitated. Brains were rapidly removed and sectioned in ice-cold cutting solution containing (in mM): 110 choline chloride, 2.5 KCl, 1.25 Na_2PO_4, 0.5 $CaCl_2$, 10 $MgSO_4$, 25 glucose, 11.6 Na-ascorbate, 3.1 Na-pyruvate, 26 $NaHCO_3$, 12 N-acetyl-L-cysteine, and 2 kynurenic acid. Horizontal (220 µm) slices

containing the LC at the level of the mesencephalic trigeminal tract neurons (ME5) were collected and transferred to a holding chamber containing artificial cerebrospinal fluid (aCSF) containing (in mM) 126 NaCl, 2.5 KCl, 1.2 $MgCl_2$, 2.4 $CaCl_2$, 1.2 NaH_2PO_4, 21.4 $NaHCO_3$, and 11.1 glucose plus 1 Na ascorbate, 1 Na pyruvate, 6 N-acetyl-L-cysteine and MK-801 to minimize excitonic effects induced by sectioning. Slices recovered for 30 min at 32°C followed by at least 30 min at room temperature prior to recording.

Slices were transferred to a recording chamber where they were perfused with warmed aCSF (inline heater, 32-34°C, Warner Instruments) at a rate of approximately 2 mL/min via gravity or a peristaltic pump (Warner Instruments). Slices were visualized under Dödt gradient contrast (DGC) optics on an upright microscope (Nikon FN1 or Zeiss Examiner D1). Putative LC-NE neurons were identified first by location (immediately medial to ME5 neurons, rostral to the fourth ventricle) and large (>20 µm) cell bodies, followed by visual presence of NM or EYFP fluorescence (controls). Electrophysiological parameters for LC-NE neuron identification included slow, irregular spontaneous action potential generation, presence of A-type potassium currents and a rebound delay after a hyperpolarizing step (-100 pA) in current clamp and low input resistance (approximately 100 MΩ, -60 V_{hold}) (Williams et al., 1984). Thin wall glass (World Precision Instruments or Warner Instruments) was used for cell-attached and whole-cell recordings, patch pipettes were pulled from thin-wall glass, and displayed resistances of 2.5-3 MΩ when filled with an intracellular solution containing (in mM): 135 K gluconate, 10 HEPES, 5 KCl, 5 $MgCl_2$, 0.1 EGTA, 0.075 $CaCl_2$, 2 ATP, 0.4 GTP, pH 7.35, liquid junction potential was calculated to be -17 mV, and was not corrected. Cell attached recordings were conducted using a Na-HEPES based intracellular solution (plus 20 mM NaCl, 290 mOsm/L, pH 7.4) (Branch and Beckstead, 2012). Frequency-current (F-I) relationships were calculated as spikes

per second across the 2 second depolarization step. Gain was calculated as the slope of the steady state F-I curve, from 0-250pA. Cell-attached frequency was calculated as spikes per second during a 30 second sweep.

Behavioral assays. Behavioral assays were performed in the following order, from least to most stressful.

Sleep latency: Latency to sleep was measured as the duration of time it took for the mouse to fall asleep following mild stimulation (gentle handling). A sleep bout was defined as 2 min of uninterrupted sleep behavior, followed by 75% of the following 8 min (Hunsley and Palmiter, 2004). This assay has been previously validated using EEG recordings (Porter-Stransky et al., 2019). Sleep testing began at 9:00 A.M., 2 h into the light cycle when mice typically engage in sleep behavior naturally. Videos were recorded for each session and scored by an experienced observer. Previous research by our group and other has revealed that increasing LC-NE transmission decreases sleep latency, while NE depletion has the opposite effect (Porter-Stransky et al., 2019).

Novelty-suppressed feeding: Chow was removed from individual home cages 24 h prior to behavioral testing. Mice were moved to the test room under red light and allowed to habituate for 2 h prior to the start of the test. Individual mice were placed in a novel arena (10” × 18” × 10”) with a single pellet of standard mouse chow located in the center. The latency to feed, operationally defined as grasping and biting the food pellet, was recorded using a stopwatch. Mice that did not feed within the 15-min period were assigned a latency score of 900 s (Tillage et al., 2020b). We have shown that increasing NE promotes anxiety-like behavior in this task reflected by longer

latencies to eat in the novel environment, while decreasing attenuates anxiety and reduces latency to eat (Lustberg et al., 2020).

Fear conditioning and context testing: Fear-conditioning training and subsequent contextual fear testing is a widely used assessment of associative memory, particularly for an environment in which an aversive stimulus (footshock) was previously administered. This method has been described previously by our group and others and is sensitive to changes in NE (Murchison et al., 2004; Chalermpalanupap et al., 2018; Butkovich et al., 2020). Mice were placed in a fear-conditioning apparatus (7 in. x 7 in. x 12 in.; Coulbourn Instruments) with a metal shock grid floor. Following 3 min of habituation, three conditioned stimulus (CS)-unconditioned stimulus (US) pairings were presented with a 1-minute intertrial interval. The CS was a 20-second, 85 dB tone which co-terminated with the US, a 2-s, 0.5 mA footshock (Precision Animal Shocker, Colbour Instruments). The following day, the context test was conducted by placing animals back into the fear conditioning chamber without the administration of CS-US pairings. Freezing behavior was measured as a readout of memory for the fear-associated context.

Statistical analyses. Cell counting and HPLC measurements of catechol concentrations were compared between hTyr-injected and control groups using a student's t-test in GraphPad Prism. Similarly, behavioral assessment relied on t-test comparison between groups for latency to feed in the novelty-suppressed feeding task and average percent freezing in the contextual fear assay. R Bioconductor packages were utilized for statistical analyses of RNA sequencing data, including differential gene expression (DGE).

Results

Viral infusion of hTyr induces NM-like pigmentation in the LC of mice. To recapitulate NM found endogenously in the human LC, we adapted a viral vector-mediated approach to drive neuronal pigmentation in rodents. TH-Cre mice were stereotaxically infused with AAV5-DIO-hTyr in the LC to drive viral expression of hTyr (**Fig. 1a**), which is known to produce pigment when introduced in rodent SN DA neurons (Carballo-Carbajal et al., 2019). We found that hTyr expression likewise drove pigmentation of the LC in Cre+ (**Fig. 1b**) but not in Cre- mice (**Fig. 1c,d**) as early as 1 week post-infusion. This pigmentation was visible by gross anatomical inspection (**Fig. 1e**) and brightfield microscopy (**Fig. 1b**). Additionally, we confirmed the presence of melanin in this pigment using Fontana-Masson staining (**Fig. 1f**). We then utilized electron microscopy to compare the pigment granules in our rodent model (**Fig. 1g**) with endogenous NM granules from 16-year-old Rhesus macaque tissue (**Fig. 1h**). Ultrastructural inspection revealed that many of the components known to reside in endogenous NM, including pheomelanin and eumelanin pigments, lipid droplets, and a double membrane, were also present in granules from our rodent model. Together, these results validate the use of hTyr expression to induce NM-like pigmentation in the mouse LC.

Pigmentation results in loss of LC fibers but not cell bodies at 1-week. We next sought to determine if rapid accumulation of NM was toxic to LC neurons. To determine whether pigmentation impacted cell body integrity at 1 week post-injection, we performed a count of TH+ and Nissl+ cells in the LC and found no difference between mice that received hTyr or EYFP virus (**Fig. 2a, b**). Given that LC fiber/terminal degeneration precedes cell body loss in AD and PD (Doppler et al., 2021a; Gilvesy et al., 2022), we also assessed NET immunoreactivity, a marker of LC dendrite, axon, and terminal integrity. Consistent with clinical data (Gilvesy et al., 2022) and

other rodent models of LC neurodegeneration (Chalermpalanupap et al., 2018; Butkovich et al., 2020), NET immunoreactivity was visibly reduced in the LC (**Fig. 2c**), as well as in the LC projections to the anterior cingulate cortex (ACC) (**Fig. 2d**) and dentate gyrus (DG) (**Fig. 2e**) of hTyr-injected mice compared to EYFP-injected controls.

Pigmentation reduces NE levels throughout the LC network and dysregulates NE turnover in the projection fields at 1 week. Given the loss of LC axons/terminals, we assessed the impact of hTyr-driven pigmentation on tissue levels of catecholamines and their metabolites (**Fig. 3**) to determine if there was a loss of NE tone in target regions. NE was dramatically reduced in the pons, where LC cell bodies reside ($t_{(10)} = 10.14$, $p < 0.0001$), as well as in the prefrontal cortex (PFC; $t_{(10)} = 7.607$, $p < 0.0001$) and hippocampus ($t_{(10)} = 9.735$, $p < 0.0001$), two of the primary projection regions of the LC. Additionally, levels of the primary NE metabolite MHPG were also reduced in the pons ($t_{(10)} = 7.532$, $p < 0.0001$), PFC ($t_{(10)} = 5.152$, $p = 0.0004$) and hippocampus ($t_{(10)} = 3.666$, $p = 0.0043$) (**Fig. 3**). Despite the reduction of total NE and MHPG, the MHPG:NE ratio, which provides an estimate of NE turnover, was significantly increased in the PFC ($t_{(10)} = 2.905$, $p = 0.0157$) and hippocampus ($t_{(10)} = 4.392$, $p = 0.0014$) compared to controls, suggesting adaptations in the LC-NE system (**Fig. 3**). Levels of other amine neuromodulators, including DA, 5-HT, and their respective metabolites, were unchanged with the exception of an increase in DA turnover (metabolite DOPAC:DA) in both the pons ($t_{(10)} = 3.288$, $p = 0.0082$) and PFC ($t_{(10)} = 2.905$, $p = 0.0157$), suggesting that dysfunction resulting from pigmentation of the LC was largely confined to the noradrenergic system at 1 week post-injection (**Table 2**).

NM-positive LC neurons are hyperactive at 1 week. Given the increase in NE turnover, we speculated that at 1 week post-viral infusion, LC neurons burdened with NM were hyperactive. Using *ex vivo* slice electrophysiology, we found that both spontaneous pacemaker (**Fig. 4a**) and current-evoked (**Fig. 4b**) firing were significantly elevated in LC neurons that contained NM from mice that received hTyr virus compared to those from mice that received EYFP virus or other controls (those that received hTyr virus but did not display visible pigment, no virus). For spontaneous firing, one-way ANOVA showed a significant difference between groups ($F_{2,149}$ = 24.02, $p < 0.0001$), and post hoc analysis revealed that the NM-containing LC neurons were hyperactive compared to EYFP controls ($q = 8.81$, $p< 0.0001$) and other controls ($q = 9.26$, $p < 0.0001$). For evoked firing, two-way ANOVA showed a main effect of treatment ($F_{1,99} = 25.35$, $p < 0.0001$), current injection ($F_{14,1386} = 236.20$, $p < 0.0001$), and a treatment x current injection interaction ($F_{14,1386} = 5.49$, $p < 0.0001$). Post hoc analysis revealed that the NM-containing LC neurons were hyperactive compared to EYFP controls at 50 pA ($t = 3.40$, $p < 0.01$), 100 pA ($t = 4.19$, $p < 0.001$), 140 pA ($t = 4.74$, $p < 0.0001$), 180 pA ($t = 5.46$, $p < 0.0001$), 220 pA ($t = 5.27$, $p < 0.0001$), 260 pA ($t = 5.69$, $p < 0.0001$), 300 pA ($t = 4.86$, $p < 0.0001$), 340 pA ($t = 4.59$, $p < 0.0001$), 380 pA ($t = 3.82$, $p < 0.01$), and 500 pA ($t = 2.69$, $p < 0.05$).

The presence of LC pigment drives novelty-induced anxiety behavior at 1 week. Several prodromal symptoms of PD are regulated by the LC-NE system, and thus are sensitive to the early LC dysfunction which precedes neurodegeneration (Weinshenker, 2018). In particular, we have shown that LC hyperactivity and/or NE signaling is associated with increased anxiety-like behavior in rodent models of AD and PD (Butkovich et al., 2020; Kelberman et al., 2022; Iannitelli et al., 2023b; Kelberman et al., 2023). We assessed the impact of hTyr-induced pigmentation on

LC-associated behaviors, including novelty-induced anxiety, arousal, and cognition, at 1 week post-viral infusion. Consistent with the LC hyperactivity phenotype, we found that hTyr-injected mice were significantly more reactive in the novelty-suppressed feeding task, a novelty-induced stress paradigm commonly used to model anxiety that is sensitive to changes in LC-NE transmission . hTyr-expressing mice took significantly longer than EYFP controls to consume food in the novelty-suppressed feeding task ($t_{(24)} = 2.359$, $p < 0.05$) (**Fig. 5a**). Five hTyr-injected mice (approximately one third) timed out of the task at 15-min, while only one EYFP control mouse timed out of the task, further illustrating an increase in novelty-induced anxiety-like behavior resulting from LC pigmentation. Importantly, hTyr- and EYFP-injected mice displayed no differences in latency to eat in the home cage (data not shown), indicating the experimental group's increased latency to eat during the task resulted from novelty stress behavior rather than changes in satiety state. There were no differences in arousal, as measured by latency to fall asleep following gentle handling (**Fig. 5b**) or associative memory, as measured by freezing in a footshock-associated context (**Fig. 5c**).

hTyr-induced pigmentation alters the LC transcriptome at 1 week. To determine how the LC responded to NM accumulation and identify potential factors contributing to its hyperactivity and fiber degeneration, we assessed the LC-NE transcriptome using TRAP. Following confirmation of LC-mRNA enrichment with TRAP (**Fig. 6a**), we performed a gene set enrichment analysis (GSEA) to compare the gene expression patterns of our data with repositories of known gene sets. A volcano plot of differentially expressed genes is shown in **Fig. 6b**. We identified 10 KEGG pathways that were significantly enriched in the LC of hTyr-expressing animals, including Tyrosine metabolism (enrichment score (ES) = 0.622, p = 0.008), Tryptophan metabolism (ES =

0.596, p = 0.014), P53 stress signaling (ES = 0.513, p = 0.018), and lysosome activity (ES = 0.348, p = 0.042) (**Fig. 6c**).

Comparing our gene set to the Human Phenotype Ontology pathways, we found that hTyr samples displayed significant upregulation in the gene sets titled "Parkinsonism with favorable response to dopaminergic medication" (ES = 0.538, p = 0.039), "startle response" (ES = 0.558, p = 0.047), "speech articulation" (ES = 0.581, p = 0.04), and "sleep apnea" (ES = 0.591, p = 0.021) (**Fig. 6**).

The most significant transcriptional differences were seen when comparing our dataset to the Gene Ontology Biological Process gene sets. We found a staggering 140 gene sets significantly enriched in our hTyr group compared to EYFP controls. These pathways fell into four notable categories: apoptotic pathways, immune regulation, endoplasmic reticulum functioning, and heavy metal ion metabolism. Of these many upregulated pathways, we identified several that we predict are key regulators of NM-induced damage. Of particular interest were the gene sets titled "antigen processing and presentation via MHC class I" (ES = 0.74, p < 0.000), "response to iron ion" (ES = 0.61, p = 0.018), "positive regulation of macroautophagy" (ES = 0.47, p = 0.011), and "pigment metabolic process" (ES = 0.46, p = 0.024) (**Fig. 6c**).

Finally, a comparison with the Gene Ontology Cell Component database showed 9 gene sets significantly enriched in the hTyr group compared to controls. The most notable was "pigment granule" (ES = 0.434, p < 0.000), with our rodent model displaying 45 core enriched genes of the 88 total present in the gene set (**Fig. 6c**).

Persistent pigment accumulation results in neurodegeneration and neuroinflammation in the LC.

To assess the consequences of prolonged pigment burden in the LC, we allowed mice to age for several weeks following viral infusion. By 6-10 weeks, we observed a catastrophic loss of LC cell bodies and dendrites, as measured by TH immunoreactivity (**Fig. 7**). The most densely pigmented sub-regions of the LC displayed the most profound cell loss, recapitulating the pattern of neurodegeneration reported in PD (Mann and Yates, 1983a). This neurodegeneration was accompanied by a profound increase in GFAP immunoreactivity, indicating that astrocytes were reacting to and infiltrating the space vacated by dying NE neurons. Although only a few LC neurons remain at these time points, pigmented granules persisted in the LC region and were also visible beyond its typical confines. Taken together, these data suggest that pigmented granules persist following the death of their host neurons, and in fact may spread to adjacent tissue.

To more fully characterize the ultrastructural composition and distribution of NM in this model over time, we performed electron microscopy on LC tissue. As previously reported for natural human NM, the hTyr-induced NM aggregates were characterized as clusters made up of irregularly shaped granules of various electron density and sizes and lipid droplets. Overall, the clusters of NM were found in neuronal cell bodies (**Fig. 8a,c**), large membrane-delimited neuropil aggregates (**Fig. 8b,d,f**), and glial cells (**Fig. 8e,g**). To determine the phenotype of the neuronal profiles that contained NM, some sections were immunostained for TH to mark LC-NE neurons, while others were labeled for either the astrocytic marker GFAP or the microglia marker IBA-1. As shown in **Fig. 8c**, some TH-positive cell bodies and dendritic profiles were enriched in NM, confirming that NM is found within noradrenergic neurons in the LC. Regarding glial expression, our observations revealed clear examples of NM aggregates within IBA-1-positive microglia cell bodies (**Fig. 8e,g**), but not in GFAP-positive astrocytes (**Fig. 8f**). However, in some instances, GFAP-positive processes were closely apposed to NM-containing

profiles (**Fig.8f**). We speculated that the persistence of NM in the LC region after many of the NE neurons were lost could be explained by glial engulfment. To test this idea, we counted the total number of neuronal and glial profiles that contained NM in the tissue and calculated the ratio of glia:neuron profile labeling. As shown in **Fig. 8h**, this ratio increased with the length of the post-viral infusion period, from ~5% at 1 week to ~25% at 10 weeks. These data suggest that NM initially accumulates in LC-NE neurons, but gradually invades the LC neuropil following release upon neuronal death, where it is engulfed by microglia. NM was absent in controls (i.e. mice that received EYFP virus or no virus; **Fig. 8h** and data not shown). One limitation of our analysis is that because much of the NM was associated with degenerating neuronal elements (e.g. dendrites) at later time points, it was difficult to discern "intracellular" vs "extracellular" localization with confidence. Given that most of the LC-NE neurons were dead by 6-10 weeks, we assume that much of it was no longer associated with intact cells and was accessible to invading glial at these time points.

Loss of pigment-bearing noradrenergic neurons depletes catecholamine levels in the LC and projection regions and dysregulates NE turnover.

Following pigment-mediated LC degeneration at 6 weeks post-infusion, we re-assessed tissue catecholamine levels. In line with the 1-week data, we found an even greater decrease in NE in the pons ($t_{(9)}$ = 10.23, $p < 0.0001$;), PFC ($t_{(9)}$ = 9.745, $p < 0.0001$), and hippocampus ($t_{(9)}$ = 12.83, < 0.0001) of hTyr-injected mice as compared to EYFP controls (**Fig. 9**). Similarly, we found a decrease in MHPG in the pons ($t_{(9)}$ = 9.489, $p < 0.0001$), PFC ($t_{(9)}$ = 7.659, $p < 0.0001$), and hippocampus ($t_{(9)}$ = 8.207, $p < 0.0001$) (**Fig. 9**). While NE turnover (MHPG:NE) was decreased in the pons ($t_{(9)}$ = 4.427, $p = 0.0017$), the increased NE turnover seen in projection regions at 1 week

persisted in the PFC ($t_{(9)}$ = 3.11, p = 0.0125) and hippocampus ($t_{(9)}$ = 2.697, p = 0.0245) at 6 weeks (**Fig. 9**). Furthermore, DA turnover was increased in the hippocampus of hTyr-injected animals ($t_{(9)}$ = 2.623, p = 0.0277), likely driven by an increase of the metabolite DOPAC ($t_{(9)}$ = 3.079, p = 0.0132). No changes in 5-HT, metabolite 5-HIAA, or turnover was found in any region at 6 weeks (**Table 2**).

Pigment-mediated neurodegeneration has no behavioral effects at 6-10 weeks. Despite the catastrophic loss of LC neurons and decrease in neurotransmitter levels at 6-10 weeks in mice with NM accumulation, we did not observe any significant differences in behavior compared to mice that received EYFP virus. Notably, novelty-induced anxiety, which was increased in hTyr mice at 1-week, did not differ statistically between groups at 6- or 10-weeks (**Fig. 10a,d**). Pigment-expressing mice also displayed no differences in sleep latency (**Fig. 10b,e**) or contextual fear conditioning (**Fig. 10c,f**).

Discussion

The present study characterized the impact of hTyr-induced pigment in the LC of mice, allowing the determineation of causal relationships between NM accumulation in noradrenergic neurons, LC-NE integrity, and the development of non-motor symptoms reminiscent of prodromal AD and PD in humans. The expression of pigmentation driven by viral delivery of hTyr is consistent with prior work focused on the SN (Carballo-Carbajal et al., 2019). In our model, neuronal dysfunction is evident as early as 1-week post-infusion. Even at this early time point, we found no difference in the number of noradrenergic or total LC cell bodies, as but dramatically decreased NET immunoreactivity in the pons, PFC, and hippocampus of hTyr mice compared to controls,

suggesting loss of fiber/terminal integrity. These findings are consistent with other reports of early LC axon loss in neurodegenerative diseases (Weinshenker, 2018; Doppler et al., 2021b; Gilvesy et al., 2022). Concurrent with fiber loss was a depletion of NE and its primary metabolite MHPG in the hippocampus and PFC. We also found elevated MHPG:NE ratio, a well validated measure of NE turnover, in projection regions, suggesting increased release from surviving LC fibers. This feature has been described in other rodent models of LC neurodegeneration (Hallman and Jonsson, 1984; Iannitelli et al., 2022) and is also consistent with LC neurodegeneration in humans (Francis et al., 1985; Raskind et al., 1999; Jacobs et al., 2021). Using a slice electrophysiology approach, we further found that LC-NE neurons containing NM were hyperactive at the cell body, including increases in both spontaneous and evoked firing. Excessive NE transmission is a common feature of compromised LC neurons, and can occur at the cell body, terminal, and/or postsynaptic receptor level, depending on the nature of the insult (Butkovich et al., 2020; Kelly et al., 2021; Iannitelli et al., 2023b; Kelberman et al., 2023). We speculate that this hyperactivity is not a direct result of pathology per se, but rather a compensatory response to damage in an effort to maintain normal NE transmission, reminiscent of compensatory LC hyperactivity following chronic inhibition by opioids (Maldonado, 1997; Mazei-Robison and Nestler, 2012). Whether the underlying compensatory mechanisms are similar (for opioids it involves upregulation of the intracellular cAMP pathway and increased excitatory drive onto LC-NE neurons) remains to be determined.

A NE hyperactivity phenotype is congruent with the LC dysfunction seen in prodromal AD and PD (Weinshenker, 2018). NM-expressing mice displayed elevated novelty-induced anxiety-like behavior at 1 week, indicating that the compensatory LC-NE hyperactivity has behavioral consequences (Lustberg et al., 2020; Kelberman et al., 2022; Iannitelli et al., 2023b). The disappearance of the anxiety phenotype at later time points when the LC was completely

degenerated is consistent with this interpretation. It was somewhat surprising that there was no effect on this hyperactivity on sleep latency, as NE transmission promotes arousal (Carter et al., 2010; Porter-Stransky et al., 2019; Poe et al., 2020). Sleep is a complex process controlled by many brain regions and neurotransmitters, and it is possible that other circuits are compensating in response to the LC hyperactivity in this case.

On a molecular level, we found that hTyr expression led to the upregulation of several important pathways. Isolation of LC-mRNA with TRAP yielded several hundred genes dysregulated between hTyr and EYFP controls. While many of these genes were significantly – but not robustly on a fold-change level – dysregulated on an individual level, pathway analyses revealed these subtle changes may have a concomitant impact on cellular health and functioning. Unsurprisingly, metabolism of the amino acids tyrosine and tryptophan, in addition to the metabolism of DA itself, were highly enriched in pigmented LC neurons. Similar increases were seen in macroautophagy and lysosome activity, indicating a cellular attempt to clear granules from the cytosol. Importantly, lysosomal dysfunction has been closely linked to PD (Nguyen et al., 2019). The upregulation of several additional pathways was directly linked to the production of pigment granules. These include increases in peroxisome activity (involved in oxidation), the response to heavy metal ions iron and manganese, and in the pigment metabolic process and pigment granule formation.

Perhaps the most intriguing results from our pathway analyses were the upregulation of specific stress response systems, immune reactions, and subsequent apoptosis in pigmented neurons. Reliable increases in P53 signaling pathways were found throughout each of our analyses, indicating severe cellular stress. Endoplasmic reticulum stress was also a consistent finding in the gene ontology biological processes analysis, revealing that cellular pigment has a severe impact

on the crucial function that the endoplasmic reticulum plays in calcium storage, protein synthesis and lipid metabolism. Antigen presentation via MHC-I was the most enriched pathway in all of our analyses, providing a clue about how LC neurons respond to pigment burden. The primary function of MHC-I is to present endogenous particles to signal cytotoxic T-cells, an intervention which leads to cellular destruction. Remarkably, catecholamine neurons are the only neurons known to express MHC-I (Cebrian et al., 2014), providing a tantalizing link between the unique possession of NM and a mechanism for dealing with this burden once it becomes harmful to the cell. In line with this theory, several apoptotic and cell-death-related pathways were also upregulated in our analyses. While these preliminary transcriptomic analyses are informative, further investigation into the specific genes driving these pathway changes is warranted. However, these findings provide preliminary evidence of potential links between our rodent model LC pigmentation and real PD-related symptoms seen in human patients.

Substantial cell death and neuroinflammation in the LC were evident by 6-10 weeks post-viral infusion, reminiscent of the consequences of hTyr overexpression in the rat substantia nigra (Carballo-Carbajal et al., 2019). Dense NM persisted in the region even when the LC was almost completely degenerated, suggesting that it had been released by dying neurons and was either extracellular or had been taken up by other cells. At the gross immunofluorescent level, the astrocyte response was dominant, but while electron microscopic analysis showed many astrocyte processes closely apposed to NM granules, only microglia appeared competent to engulf the NM. Extracellular NM-induced activation of microglia has been reported in human postmortem tissue, animal models, and cell culture (Zecca et al., 2003; Zecca et al., 2008a; Zhang et al., 2011). Neuroinflammation is a well-appreciated aspect of AD and PD that is influenced by the LC-NE system (Chalermpalanupap et al., 2013; Feinstein et al., 2016; Giorgi et al., 2020; Mercan and

Heneka, 2022; Tansey et al., 2022). Our data suggest that the release of pigmentation from degenerating LC neurons contributes to the neuroimmune response.

Due to the catastrophic loss of NE cell bodies and deteriorating state of the ones that persisted, we were unable to directly assess LC activity at the 6-10 week time points. Using HPLC as a proxy, we found increased NE turnover in LC terminal regions at 6 weeks suggestive of compensatory NE release from surviving terminals, similar to the 1 week data. However, this did not correspond with increases in anxiety-like behavior, presumably because NE, which is required for novelty-suppressed feeding (Lustberg et al., 2020), was barely above the limit of detection. There were no differences between groups in sleep latency, novelty-induced anxiety, or contextual fear memory. The loss of an anxiety-like phenotype at 6-weeks may be explained by a near-total loss of LC-NE, which is required for this behavior (Lustberg et al., 2020). While contextual fear memory should also require LC innervation of the hippocampus (McGaugh, 2013), recent studies have also implicated DA in hippocampal function and fear memory (Likhtik and Johansen, 2019; Stubbendorff and Stevenson, 2021). Thus, the increase in DA turnover in the hippocampus at 6-weeks may account for the lack of behavioral differences observed in the contextual fear task.

The present study provides novel insights into the consequences of NM accumulation in rodent LC-NE neurons. We found that pigment expression dysregulates LC neurons on a cellular and molecular level at 1 week, triggering an anxiety-like phenotype reminiscent of prodromal AD and PD. As the pigment accumulates, immune response and neurodegeneration ensue. By 6-10 weeks post-infusion, the LC has nearly entirely degenerated and most of the NM is contained in deteriorating neuronal elements, the extracellular neuropil, and microglia. An important aspect of our study is that hTyr overexpression drives extremely rapid NM accumulation (weeks) compared to natural NM accumulation in humans (decades), which likely dramatically accelerates its ability

to overwhelm cellular machinery and lead to cell death. In this respect, our approach shares the same limitation as all rodent models of neurodegenerative disease. Nevertheless, there is ample evidence that the same processes contribute to LC neuron dysregulation and demise in AD and PD. For example, LC neurons with the highest NM content are disproportionally lost in PD (Mann and Yates, 1983a). It was previously reported that hTyr-expressing SN-DA neurons took many months to degenerate (Carballo-Carbajal et al., 2019). It is not clear whether this reflects differences with our model in the virus itself (AAV2 vs Cre-dependent AAV5), species (rat vs mouse), or a true greater vulnerability of LC neurons. Thus, direct comparisons will be needed to answer this question. Ultimately, this model of pigment induction in rodent catecholamine neurons may be critical for uncovering the role NM plays in the early vulnerability of LC neurons in AD and PD.

Author Contributions

A.F.I. designed and performed research, analyzed data, and wrote the manuscript. L.H. designed and performed researched, analyzed data, and edited the manuscript. B.M. assisted with research design and data analysis. H.E.B. performed research and analyzed data. L.C.L. assisted with research design and analysis. A.L.S. performed research and analyzed data. J-F.P. performed research and analyzed data. A.S. performed research and analyzed data. S.A.S. assisted with research design and data analysis. K.M. assisted with data analysis. K.E.M. performed research and analyzed data. J.D.D. assisted with research design and contributed analytic tools. Y.S. assisted with research design and data analysis. M.J.B. designed and performed research, analyzed data, and wrote the manuscript. D.W. designed research, analyzed data, and wrote the manuscript.

Acknowledgements

This work was supported by a National Institutes of Health (NIH) National Institute of Environmental Health Sciences Training Grant (ES12870) and a NIH D-SPAN F99/K00 Award from the National Institute of Neurological Disorders and Stroke (NS129168) to A.F.I, as well as RF1 awards from the National Institute on Aging (AG079199 to D.W. and AG061175 to D.W. and M.J.B.). This study was supported in part by the Emory HPLC Bioanalytical Core (EHBC), which is subsidized by the Emory University School of Medicine and is one of the Emory Integrated Core Facilities. Additional support was provided by the Georgia Clinical & Translational Science Alliance of the National Institutes of Health under Award Number UL1TR002378. We thank Dr. M. McGuirk Sampson for assistance with R code for analysis.

References

Barden H, Levine S (1983) Histochemical observations on rodent brain melanin. Brain Res Bull 10:847-851.

Bondareff W, Mountjoy CQ, Roth M (1982) Loss of neurons of origin of the adrenergic projection to cerebral cortex (nucleus locus ceruleus) in senile dementia. Neurology 32:164-168.

Braak E, Sandmann-Keil D, Rub U, Gai WP, de Vos RA, Steur EN, Arai K, Braak H (2001) alpha-synuclein immunopositive Parkinson's disease-related inclusion bodies in lower brain stem nuclei. Acta Neuropathol 101:195-201.

Braak H, Del Tredici K (2011a) The pathological process underlying Alzheimer's disease in individuals under thirty. Acta Neuropathol 121:171-181.

Braak H, Del Tredici K (2011b) Alzheimer's pathogenesis: is there neuron-to-neuron propagation? Acta Neuropathol 121:589-595.

Braak H, Thal DR, Ghebremedhin E, Del Tredici K (2011) Stages of the pathologic process in Alzheimer disease: age categories from 1 to 100 years. J Neuropathol Exp Neurol 70:960-969.

Branch SY, Beckstead MJ (2012) Methamphetamine produces bidirectional, concentration-dependent effects on dopamine neuron excitability and dopamine-mediated synaptic currents. J Neurophysiol 108:802-809.

Bueicheku E, Diez I, Kim CM, Becker JA, Koops EA, Kwong K, Papp KV, Salat DH, Bennett DA, Rentz DM, Sperling RA, Johnson KA, Sepulcre J, Jacobs HIL (2024) Spatiotemporal patterns of locus coeruleus integrity predict cortical tau and cognition. Nat Aging 4:625-637.

Bush WD, Garguilo J, Zucca FA, Albertini A, Zecca L, Edwards GS, Nemanich RJ, Simon JD (2006) The surface oxidation potential of human neuromelanin reveals a spherical architecture with a pheomelanin core and a eumelanin surface. Proc Natl Acad Sci U S A 103:14785-14789.

Butkovich LM, Houser MC, Chalermpalanupap T, Porter-Stransky KA, Iannitelli AF, Boles JS, Lloyd GM, Coomes AS, Eidson LN, De Sousa Rodrigues ME, Oliver DL, Kelly SD, Chang J, Bengoa-Vergniory N, Wade-Martins R, Giasson BI, Joers V, Weinshenker D, Tansey MG (2020) Transgenic Mice Expressing Human alpha-Synuclein in Noradrenergic Neurons Develop Locus Ceruleus Pathology and Nonmotor Features of Parkinson's Disease. J Neurosci 40:7559-7576.

Carballo-Carbajal I, Laguna A, Romero-Gimenez J, Cuadros T, Bove J, Martinez-Vicente M, Parent A, Gonzalez-Sepulveda M, Penuelas N, Torra A, Rodriguez-Galvan B, Ballabio A, Hasegawa T, Bortolozzi A, Gelpi E, Vila M (2019) Brain tyrosinase overexpression implicates age-dependent neuromelanin production in Parkinson's disease pathogenesis. Nat Commun 10:973.

Carter ME, Yizhar O, Chikahisa S, Nguyen H, Adamantidis A, Nishino S, Deisseroth K, de Lecea L (2010) Tuning arousal with optogenetic modulation of locus coeruleus neurons. Nat Neurosci 13:1526-1533.

Cebrian C, Zucca FA, Mauri P, Steinbeck JA, Studer L, Scherzer CR, Kanter E, Budhu S, Mandelbaum J, Vonsattel JP, Zecca L, Loike JD, Sulzer D (2014) MHC-I expression renders catecholaminergic neurons susceptible to T-cell-mediated degeneration. Nat Commun 5:3633.

Chalermpalanupap T, Schroeder JP, Rorabaugh JM, Liles LC, Lah JJ, Levey AI, Weinshenker D (2018) Locus Coeruleus Ablation Exacerbates Cognitive Deficits, Neuropathology, and Lethality in P301S Tau Transgenic Mice. J Neurosci 38:74-92.

Chalermpalanupap T, Kinkead B, Hu WT, Kummer MP, Hammerschmidt T, Heneka MT, Weinshenker D, Levey AI (2013) Targeting norepinephrine in mild cognitive impairment and Alzheimer's disease. Alzheimers Res Ther 5:21.

Del Tredici K, Rub U, De Vos RA, Bohl JR, Braak H (2002) Where does parkinson disease pathology begin in the brain? J Neuropathol Exp Neurol 61:413-426.

DeMattei M, Levi AC, Fariello RG (1986) Neuromelanic pigment in substantia nigra neurons of rats and dogs. Neurosci Lett 72:37-42.

Dexter DT, Jenner P, Schapira AH, Marsden CD (1992) Alterations in levels of iron, ferritin, and other trace metals in neurodegenerative diseases affecting the basal ganglia. The Royal Kings and Queens Parkinson's Disease Research Group. Ann Neurol 32 Suppl:S94-100.

Doppler CEJ, Kinnerup MB, Brune C, Farrher E, Betts M, Fedorova TD, Schaldemose JL, Knudsen K, Ismail R, Seger AD, Hansen AK, Staer K, Fink GR, Brooks DJ, Nahimi A, Borghammer P, Sommerauer M (2021a) Regional locus coeruleus degeneration is uncoupled from noradrenergic terminal loss in Parkinson's disease. Brain 144:2732-2744.

Doppler CEJ, Kinnerup MB, Brune C, Farrher E, Betts M, Fedorova TD, Schaldemose JL, Knudsen K, Ismail R, Seger AD, Hansen AK, Staer K, Fink GR, Brooks DJ, Nahimi A, Borghammer P, Sommerauer M (2021b) Regional locus coeruleus degeneration is uncoupled from noradrenergic terminal loss in Parkinson's disease. Brain.

Ehrenberg AJ, Suemoto CK, Franca Resende EP, Petersen C, Leite REP, Rodriguez RD, Ferretti-Rebustini REL, You M, Oh J, Nitrini R, Pasqualucci CA, Jacob-Filho W, Kramer

JH, Gatchel JR, Grinberg LT (2018) Neuropathologic Correlates of Psychiatric Symptoms in Alzheimer's Disease. J Alzheimers Dis 66:115-126.

Ehrenberg AJ, Nguy AK, Theofilas P, Dunlop S, Suemoto CK, Di Lorenzo Alho AT, Leite RP, Diehl Rodriguez R, Mejia MB, Rub U, Farfel JM, de Lucena Ferretti-Rebustini RE, Nascimento CF, Nitrini R, Pasquallucci CA, Jacob-Filho W, Miller B, Seeley WW, Heinsen H, Grinberg LT (2017) Quantifying the accretion of hyperphosphorylated tau in the locus coeruleus and dorsal raphe nucleus: the pathological building blocks of early Alzheimer's disease. Neuropathol Appl Neurobiol 43:393-408.

Falgas N, Pena-Gonzalez M, Val-Guardiola A, Perez-Millan A, Guillen N, Sarto J, Esteller D, Bosch B, Fernandez-Villullas G, Tort-Merino A, Maya G, Auge JM, Iranzo A, Balasa M, Llado A, Morales-Ruiz M, Bargallo N, Munoz-Moreno E, Grinberg LT, Sanchez-Valle R (2024) Locus coeruleus integrity and neuropsychiatric symptoms in a cohort of early- and late-onset Alzheimer's disease. Alzheimers Dement.

Feinstein DL, Kalinin S, Braun D (2016) Causes, consequences, and cures for neuroinflammation mediated via the locus coeruleus: noradrenergic signaling system. J Neurochem 139 Suppl 2:154-178.

Francis PT, Palmer AM, Sims NR, Bowen DM, Davison AN, Esiri MM, Neary D, Snowden JS, Wilcock GK (1985) Neurochemical studies of early-onset Alzheimer's disease. Possible influence on treatment. N Engl J Med 313:7-11.

German DC, Manaye KF, White CL, 3rd, Woodward DJ, McIntire DD, Smith WK, Kalaria RN, Mann DM (1992) Disease-specific patterns of locus coeruleus cell loss. Ann Neurol 32:667-676.

Ghosh A, Torraville SE, Mukherjee B, Walling SG, Martin GM, Harley CW, Yuan Q (2019) An experimental model of Braak's pretangle proposal for the origin of Alzheimer's disease: the role of locus coeruleus in early symptom development. Alzheimers Res Ther 11:59.

Gilvesy A, Husen E, Magloczky Z, Mihaly O, Hortobagyi T, Kanatani S, Heinsen H, Renier N, Hokfelt T, Mulder J, Uhlen M, Kovacs GG, Adori C (2022) Spatiotemporal characterization of cellular tau pathology in the human locus coeruleus-pericoerulear complex by three-dimensional imaging. Acta Neuropathol 144:651-676.

Giorgi FS, Biagioni F, Galgani A, Pavese N, Lazzeri G, Fornai F (2020) Locus Coeruleus Modulates Neuroinflammation in Parkinsonism and Dementia. Int J Mol Sci 21.

Hallman H, Jonsson G (1984) Monoamine neurotransmitter metabolism in microencephalic rat brain after prenatal methylazoxymethanol treatment. Brain Res Bull 13:383-389.

Heneka MT, Ramanathan M, Jacobs AH, Dumitrescu-Ozimek L, Bilkei-Gorzo A, Debeir T, Sastre M, Galldiks N, Zimmer A, Hoehn M, Heiss WD, Klockgether T, Staufenbiel M (2006) Locus ceruleus degeneration promotes Alzheimer pathogenesis in amyloid precursor protein 23 transgenic mice. J Neurosci 26:1343-1354.

Hunsley MS, Palmiter RD (2004) Altered sleep latency and arousal regulation in mice lacking norepinephrine. Pharmacol Biochem Behav 78:765-773.

Iannitelli AF, Weinshenker D (2023) Riddles in the dark: Decoding the relationship between neuromelanin and neurodegeneration in locus coeruleus neurons. Neurosci Biobehav Rev 152:105287.

Iannitelli AF, Segal A, Pare JF, Mulvey B, Liles LC, Sloan SA, McCann KE, Dougherty JD, Smith Y, Weinshenker D (2023a) Tyrosinase-induced neuromelanin accumulation triggers rapid dysregulation and degeneration of the mouse locus coeruleus. bioRxiv.

Iannitelli AF, Kelberman MA, Lustberg DJ, Korukonda A, McCann KE, Mulvey B, Segal A, Liles LC, Sloan SA, Dougherty JD, Weinshenker D (2022) The Neurotoxin DSP-4 Dysregulates the Locus Coeruleus-Norepinephrine System and Recapitulates Molecular and Behavioral Aspects of Prodromal Neurodegenerative Disease. bioRxiv:2022.2009.2027.509797.

Iannitelli AF, Kelberman MA, Lustberg DJ, Korukonda A, McCann KE, Mulvey B, Segal A, Liles LC, Sloan SA, Dougherty JD, Weinshenker D (2023b) The Neurotoxin DSP-4 Dysregulates the Locus Coeruleus-Norepinephrine System and Recapitulates Molecular and Behavioral Aspects of Prodromal Neurodegenerative Disease. eNeuro 10.

Iversen LL, Rossor MN, Reynolds GP, Hills R, Roth M, Mountjoy CQ, Foote SL, Morrison JH, Bloom FE (1983) Loss of pigmented dopamine-beta-hydroxylase positive cells from locus coeruleus in senile dementia of Alzheimer's type. Neurosci Lett 39:95-100.

Jacobs HIL, Becker JA, Kwong K, Engels-Dominguez N, Prokopiou PC, Papp KV, Properzi M, Hampton OL, d'Oleire Uquillas F, Sanchez JS, Rentz DM, El Fakhri G, Normandin MD, Price JC, Bennett DA, Sperling RA, Johnson KA (2021) In vivo and neuropathology data support locus coeruleus integrity as indicator of Alzheimer's disease pathology and cognitive decline. Sci Transl Med 13:eabj2511.

Kang SS, Liu X, Ahn EH, Xiang J, Manfredsson FP, Yang X, Luo HR, Liles LC, Weinshenker D, Ye K (2020) Norepinephrine metabolite DOPEGAL activates AEP and pathological Tau aggregation in locus coeruleus. J Clin Invest 130:422-437.

Kang SS, Meng L, Zhang X, Wu Z, Mancieri A, Xie B, Liu X, Weinshenker D, Peng J, Zhang Z, Ye K (2022) Tau modification by the norepinephrine metabolite DOPEGAL stimulates its pathology and propagation. Nat Struct Mol Biol 29:292-305.

Kelberman MA, Anderson CR, Chlan E, Rorabaugh JM, McCann KE, Weinshenker D (2022) Consequences of Hyperphosphorylated Tau in the Locus Coeruleus on Behavior and Cognition in a Rat Model of Alzheimer's Disease. J Alzheimers Dis 86:1037-1059.

Kelberman MA, Rorabaugh JM, Anderson CR, Marriott A, DePuy SD, Rasmussen K, McCann KE, Weiss JM, Weinshenker D (2023) Age-dependent dysregulation of locus coeruleus firing in a transgenic rat model of Alzheimer's disease. Neurobiol Aging 125:98-108.

Kelly L, Seifi M, Ma R, Mitchell SJ, Rudolph U, Viola KL, Klein WL, Lambert JJ, Swinny JD (2021) Identification of intraneuronal amyloid beta oligomers in locus coeruleus neurons of Alzheimer's patients and their potential impact on inhibitory neurotransmitter receptors and neuronal excitability. Neuropathol Appl Neurobiol 47:488-505.

Li Y, Wang C, Wang J, Zhou Y, Ye F, Zhang Y, Cheng X, Huang Z, Liu K, Fei G, Zhong C, Zeng M, Jin L (2019) Mild cognitive impairment in de novo Parkinson's disease: A neuromelanin MRI study in locus coeruleus. Mov Disord 34:884-892.

Likhtik E, Johansen JP (2019) Neuromodulation in circuits of aversive emotional learning. Nat Neurosci 22:1586-1597.

Lustberg D, Tillage RP, Bai Y, Pruitt M, Liles LC, Weinshenker D (2020) Noradrenergic circuits in the forebrain control affective responses to novelty. Psychopharmacology (Berl) 237:3337-3355.

Lustberg DJ, Liu JQ, Iannitelli AF, Vanderhoof SO, Liles LC, McCann KE, Weinshenker D (2022) Norepinephrine and dopamine contribute to distinct repetitive behaviors induced by novel odorant stress in male and female mice. Horm Behav 144:105205.

Maldonado R (1997) Participation of noradrenergic pathways in the expression of opiate withdrawal: biochemical and pharmacological evidence. Neurosci Biobehav Rev 21:91-104.

Mann DM, Yates PO (1974) Lipoprotein pigments--their relationship to ageing in the human nervous system. II. The melanin content of pigmented nerve cells. Brain 97:489-498.

Mann DM, Yates PO (1983a) Possible role of neuromelanin in the pathogenesis of Parkinson's disease. Mech Ageing Dev 21:193-203.

Mann DM, Yates PO (1983b) Pathological basis for neurotransmitter changes in Parkinson's disease. Neuropathol Appl Neurobiol 9:3-19.

Mann DM, Lincoln J, Yates PO, Stamp JE, Toper S (1980) Changes in the monoamine containing neurones of the human CNS in senile dementia. Br J Psychiatry 136:533-541.

Matchett BJ, Grinberg LT, Theofilas P, Murray ME (2021) The mechanistic link between selective vulnerability of the locus coeruleus and neurodegeneration in Alzheimer's disease. Acta Neuropathol 141:631-650.

Mavridis M, Degryse AD, Lategan AJ, Marien MR, Colpaert FC (1991) Effects of locus coeruleus lesions on parkinsonian signs, striatal dopamine and substantia nigra cell loss after 1-methyl-4-phenyl-1,2,3,6-tetrahydropyridine in monkeys: a possible role for the locus coeruleus in the progression of Parkinson's disease. Neuroscience 41:507-523.

Mazei-Robison MS, Nestler EJ (2012) Opiate-induced molecular and cellular plasticity of ventral tegmental area and locus coeruleus catecholamine neurons. Cold Spring Harb Perspect Med 2:a012070.

McGaugh JL (2013) Making lasting memories: remembering the significant. Proc Natl Acad Sci U S A 110 Suppl 2:10402-10407.

Mercan D, Heneka MT (2022) The Contribution of the Locus Coeruleus-Noradrenaline System Degeneration during the Progression of Alzheimer's Disease. Biology (Basel) 11.

Mootha VK et al. (2003) PGC-1alpha-responsive genes involved in oxidative phosphorylation are coordinately downregulated in human diabetes. Nat Genet 34:267-273.

Mulvey B, Bhatti DL, Gyawali S, Lake AM, Kriaucionis S, Ford CP, Bruchas MR, Heintz N, Dougherty JD (2018) Molecular and Functional Sex Differences of Noradrenergic Neurons in the Mouse Locus Coeruleus. Cell Rep 23:2225-2235.

Murchison CF, Zhang XY, Zhang WP, Ouyang M, Lee A, Thomas SA (2004) A distinct role for norepinephrine in memory retrieval. Cell 117:131-143.

Nguyen M, Wong YC, Ysselstein D, Severino A, Krainc D (2019) Synaptic, Mitochondrial, and Lysosomal Dysfunction in Parkinson's Disease. Trends Neurosci 42:140-149.

Pall HS, Williams AC, Blake DR, Lunec J, Gutteridge JM, Hall M, Taylor A (1987) Raised cerebrospinal-fluid copper concentration in Parkinson's disease. Lancet 2:238-241.

Pletnikova O, Kageyama Y, Rudow G, LaClair KD, Albert M, Crain BJ, Tian J, Fowler D, Troncoso JC (2018) The spectrum of preclinical Alzheimer's disease pathology and its modulation by ApoE genotype. Neurobiol Aging 71:72-80.

Poe GR, Foote S, Eschenko O, Johansen JP, Bouret S, Aston-Jones G, Harley CW, Manahan-Vaughan D, Weinshenker D, Valentino R, Berridge C, Chandler DJ, Waterhouse B, Sara SJ (2020) Locus coeruleus: a new look at the blue spot. Nat Rev Neurosci 21:644-659.

Porter-Stransky KA, Centanni SW, Karne SL, Odil LM, Fekir S, Wong JC, Jerome C, Mitchell HA, Escayg A, Pedersen NP, Winder DG, Mitrano DA, Weinshenker D (2019) Noradrenergic Transmission at Alpha1-Adrenergic Receptors in the Ventral Periaqueductal Gray Modulates Arousal. Biol Psychiatry 85:237-247.

Prediger RD, Matheus FC, Schwarzbold ML, Lima MM, Vital MA (2012) Anxiety in Parkinson's disease: a critical review of experimental and clinical studies. Neuropharmacology 62:115-124.

Prokopiou PC, Engels-Dominguez N, Papp KV, Scott MR, Schultz AP, Schneider C, Farrell ME, Buckley RF, Quiroz YT, El Fakhri G, Rentz DM, Sperling RA, Johnson KA, Jacobs HIL (2022) Lower novelty-related locus coeruleus function is associated with Abeta-related cognitive decline in clinically healthy individuals. Nat Commun 13:1571.

Raskind MA, Peskind ER, Holmes C, Goldstein DS (1999) Patterns of cerebrospinal fluid catechols support increased central noradrenergic responsiveness in aging and Alzheimer's disease. Biol Psychiatry 46:756-765.

Remy P, Doder M, Lees A, Turjanski N, Brooks D (2005) Depression in Parkinson's disease: loss of dopamine and noradrenaline innervation in the limbic system. Brain 128:1314-1322.

Rorabaugh JM, Chalermpalanupap T, Botz-Zapp CA, Fu VM, Lembeck NA, Cohen RM, Weinshenker D (2017) Chemogenetic locus coeruleus activation restores reversal learning in a rat model of Alzheimer's disease. Brain 140:3023-3038.

Sasaki M, Shibata E, Tohyama K, Takahashi J, Otsuka K, Tsuchiya K, Takahashi S, Ehara S, Terayama Y, Sakai A (2006) Neuromelanin magnetic resonance imaging of locus ceruleus and substantia nigra in Parkinson's disease. Neuroreport 17:1215-1218.

Sommerauer M, Fedorova TD, Hansen AK, Knudsen K, Otto M, Jeppesen J, Frederiksen Y, Blicher JU, Geday J, Nahimi A, Damholdt MF, Brooks DJ, Borghammer P (2018) Evaluation of the noradrenergic system in Parkinson's disease: an 11C-MeNER PET and neuromelanin MRI study. Brain 141:496-504.

Song S, Wang Q, Jiang L, Oyarzabal E, Riddick NV, Wilson B, Moy SS, Shih YI, Hong JS (2019) Noradrenergic dysfunction accelerates LPS-elicited inflammation-related ascending sequential neurodegeneration and deficits in non-motor/motor functions. Brain Behav Immun 81:374-387.

Srinivasan J, Schmidt WJ (2003) Potentiation of parkinsonian symptoms by depletion of locus coeruleus noradrenaline in 6-hydroxydopamine-induced partial degeneration of substantia nigra in rats. Eur J Neurosci 17:2586-2592.

Stubbendorff C, Stevenson CW (2021) Dopamine regulation of contextual fear and associated neural circuit function. Eur J Neurosci 54:6933-6947.

Subramanian A, Tamayo P, Mootha VK, Mukherjee S, Ebert BL, Gillette MA, Paulovich A, Pomeroy SL, Golub TR, Lander ES, Mesirov JP (2005) Gene set enrichment analysis: a knowledge-based approach for interpreting genome-wide expression profiles. Proc Natl Acad Sci U S A 102:15545-15550.

Sulzer D, Mosharov E, Talloczy Z, Zucca FA, Simon JD, Zecca L (2008) Neuronal pigmented autophagic vacuoles: lipofuscin, neuromelanin, and ceroid as macroautophagic responses during aging and disease. J Neurochem 106:24-36.

Sulzer D, Bogulavsky J, Larsen KE, Behr G, Karatekin E, Kleinman MH, Turro N, Krantz D, Edwards RH, Greene LA, Zecca L (2000) Neuromelanin biosynthesis is driven by excess cytosolic catecholamines not accumulated by synaptic vesicles. Proc Natl Acad Sci U S A 97:11869-11874.

Tansey MG, Wallings RL, Houser MC, Herrick MK, Keating CE, Joers V (2022) Inflammation and immune dysfunction in Parkinson disease. Nat Rev Immunol 22:657-673.

Theofilas P, Ehrenberg AJ, Dunlop S, Di Lorenzo Alho AT, Nguy A, Leite REP, Rodriguez RD, Mejia MB, Suemoto CK, Ferretti-Rebustini REL, Polichiso L, Nascimento CF, Seeley WW, Nitrini R, Pasqualucci CA, Jacob Filho W, Rueb U, Neuhaus J, Heinsen H, Grinberg LT (2017) Locus coeruleus volume and cell population changes during Alzheimer's disease progression: A stereological study in human postmortem brains with potential implication for early-stage biomarker discovery. Alzheimers Dement 13:236-246.

Tillage RP, Wilson GE, Liles LC, Holmes PV, Weinshenker D (2020a) Chronic Environmental or Genetic Elevation of Galanin in Noradrenergic Neurons Confers Stress Resilience in Mice. J Neurosci 40:7464-7474.

Tillage RP, Sciolino NR, Plummer NW, Lustberg D, Liles LC, Hsiang M, Powell JM, Smith KG, Jensen P, Weinshenker D (2020b) Elimination of galanin synthesis in noradrenergic neurons reduces galanin in select brain areas and promotes active coping behaviors. Brain Struct Funct 225:785-803.

Vazey EM, Aston-Jones G (2012) The emerging role of norepinephrine in cognitive dysfunctions of Parkinson's disease. Front Behav Neurosci 6:48.

Weinshenker D (2018) Long Road to Ruin: Noradrenergic Dysfunction in Neurodegenerative Disease. Trends Neurosci 41:211-223.

Williams JT, North RA, Shefner SA, Nishi S, Egan TM (1984) Membrane properties of rat locus coeruleus neurones. Neuroscience 13:137-156.

Ye R, O'Callaghan C, Rua C, Hezemans FH, Holland N, Malpetti M, Jones PS, Barker RA, Williams-Gray CH, Robbins TW, Passamonti L, Rowe J (2022) Locus Coeruleus

Integrity from 7 T MRI Relates to Apathy and Cognition in Parkinsonian Disorders. Mov Disord 37:1663-1672.

Zarow C, Lyness SA, Mortimer JA, Chui HC (2003) Neuronal loss is greater in the locus coeruleus than nucleus basalis and substantia nigra in Alzheimer and Parkinson diseases. Arch Neurol 60:337-341.

Zecca L, Zucca FA, Wilms H, Sulzer D (2003) Neuromelanin of the substantia nigra: a neuronal black hole with protective and toxic characteristics. Trends Neurosci 26:578-580.

Zecca L, Wilms H, Geick S, Claasen JH, Brandenburg LO, Holzknecht C, Panizza ML, Zucca FA, Deuschl G, Sievers J, Lucius R (2008a) Human neuromelanin induces neuroinflammation and neurodegeneration in the rat substantia nigra: implications for Parkinson's disease. Acta Neuropathol 116:47-55.

Zecca L, Stroppolo A, Gatti A, Tampellini D, Toscani M, Gallorini M, Giaveri G, Arosio P, Santambrogio P, Fariello RG, Karatekin E, Kleinman MH, Turro N, Hornykiewicz O, Zucca FA (2004) The role of iron and copper molecules in the neuronal vulnerability of locus coeruleus and substantia nigra during aging. Proc Natl Acad Sci U S A 101:9843-9848.

Zecca L, Bellei C, Costi P, Albertini A, Monzani E, Casella L, Gallorini M, Bergamaschi L, Moscatelli A, Turro NJ, Eisner M, Crippa PR, Ito S, Wakamatsu K, Bush WD, Ward WC, Simon JD, Zucca FA (2008b) New melanic pigments in the human brain that accumulate in aging and block environmental toxic metals. Proc Natl Acad Sci U S A 105:17567-17572.

Zhang W, Phillips K, Wielgus AR, Liu J, Albertini A, Zucca FA, Faust R, Qian SY, Miller DS, Chignell CF, Wilson B, Jackson-Lewis V, Przedborski S, Joset D, Loike J, Hong JS,

Sulzer D, Zecca L (2011) Neuromelanin activates microglia and induces degeneration of dopaminergic neurons: implications for progression of Parkinson's disease. Neurotox Res 19:63-72.

Zweig RM, Cardillo JE, Cohen M, Giere S, Hedreen JC (1993) The locus ceruleus and dementia in Parkinson's disease. Neurology 43:986-991.

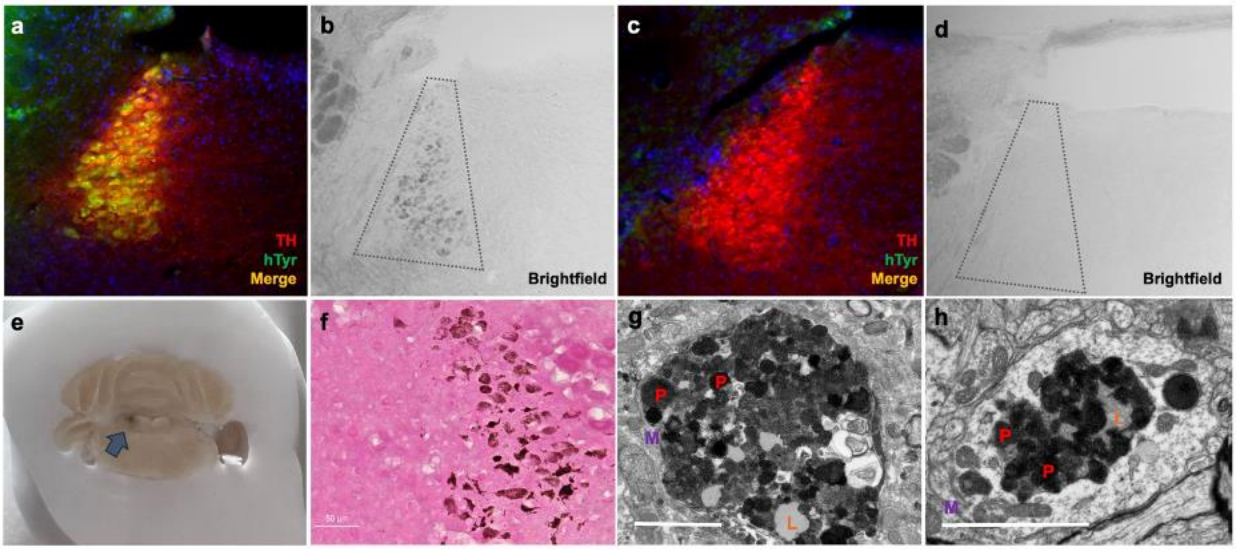

Fig. 1. hTyr induces pigmentation in the LC reminiscent of endogenous NM at 1 week. Mice received stereotaxic injection of AAV5-DIO-hTyr into the LC, driving expression of human tyrosinase in TH-Cre+ experimental animals (**a**) but not in TH-Cre- controls (**c**). Although rodents (TH-Cre- image shown here) do not display endogenous NM (**d**), the expression of hTyr resulted in LC pigmentation visible by brightfield microscopy (**b**) and gross anatomical inspection (arrow) (**e**). This hTyr-derived pigment stained positive for melanin components with Fontana-Masson (**f**), and electron microscopic analysis of these granules (**g**) showed they contain several features characteristic of endogenous NM from aged rhesus macaques (**h**), including pigment of various shades (P, red), lipid droplets (L, orange), and enclosure in a membrane (M, purple). Scale bar = 5 μM. Immunofluorescent and brightfield images (A-D, F) were acquired at 20x magnification.

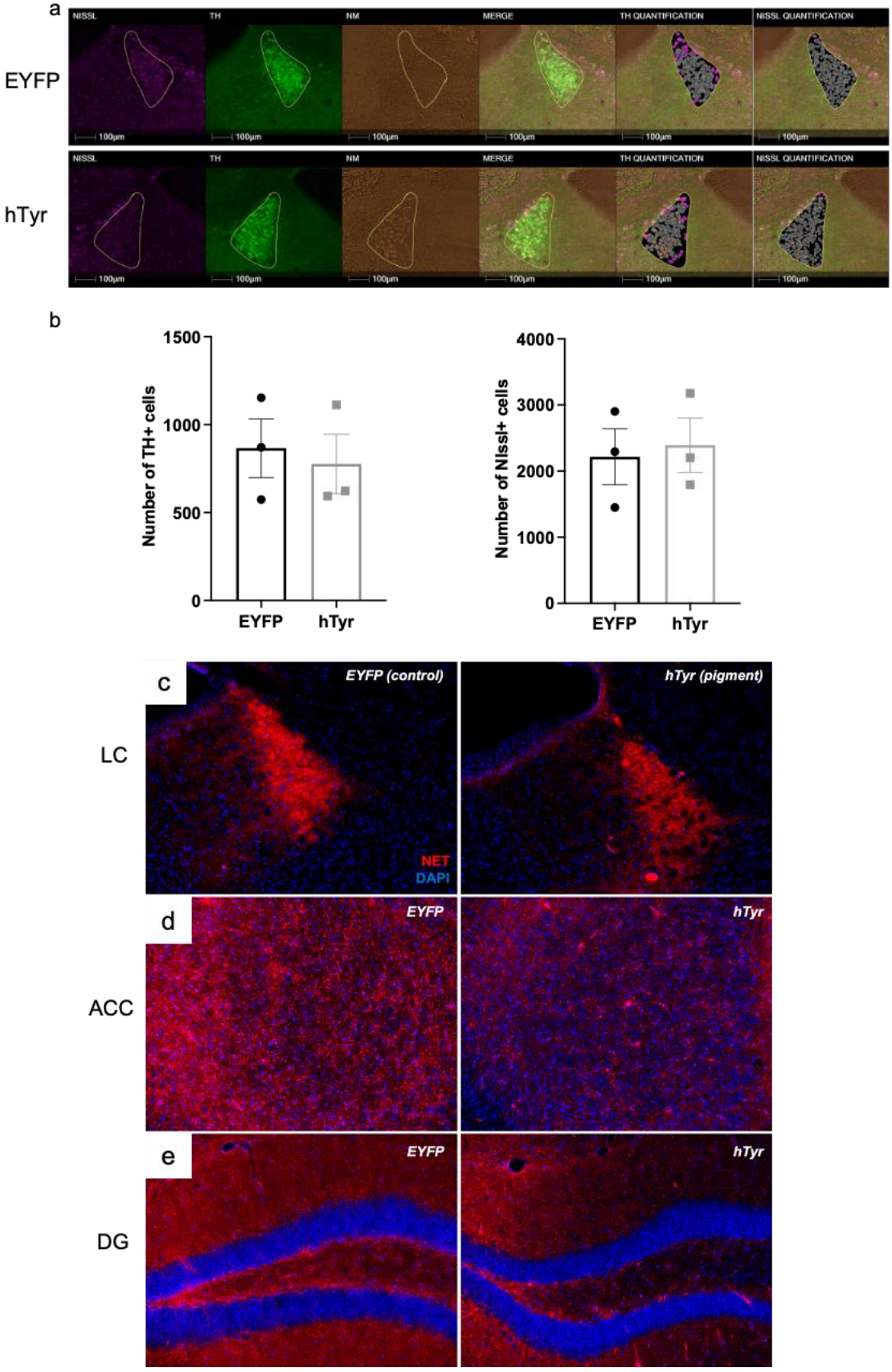

Fig. 2. The presence of NM-like pigmentation results in loss of LC fibers but not cell bodies at 1-week. TH-Cre mice received LC infusion of AAV5-DIO-hTyr or EYFP control and were assessed for LC neuron damage 1 week later. hTyr-induced NM expression did not alter LC neuron number (TH+ or Nissl+ cells). Representative immunofluorescent HALO images are shown in (**a)**, quantification (mean ± SEM) shown in (**b**). NM accumulation resulted in substantial loss of axon terminals as measured by NE transporter (NET, red; DAPI, blue) immunoreactivity in the anterior cingulate cortex (ACC) (**c**) and dentate gyrus (DG) (**d**). Images acquired at 20X.

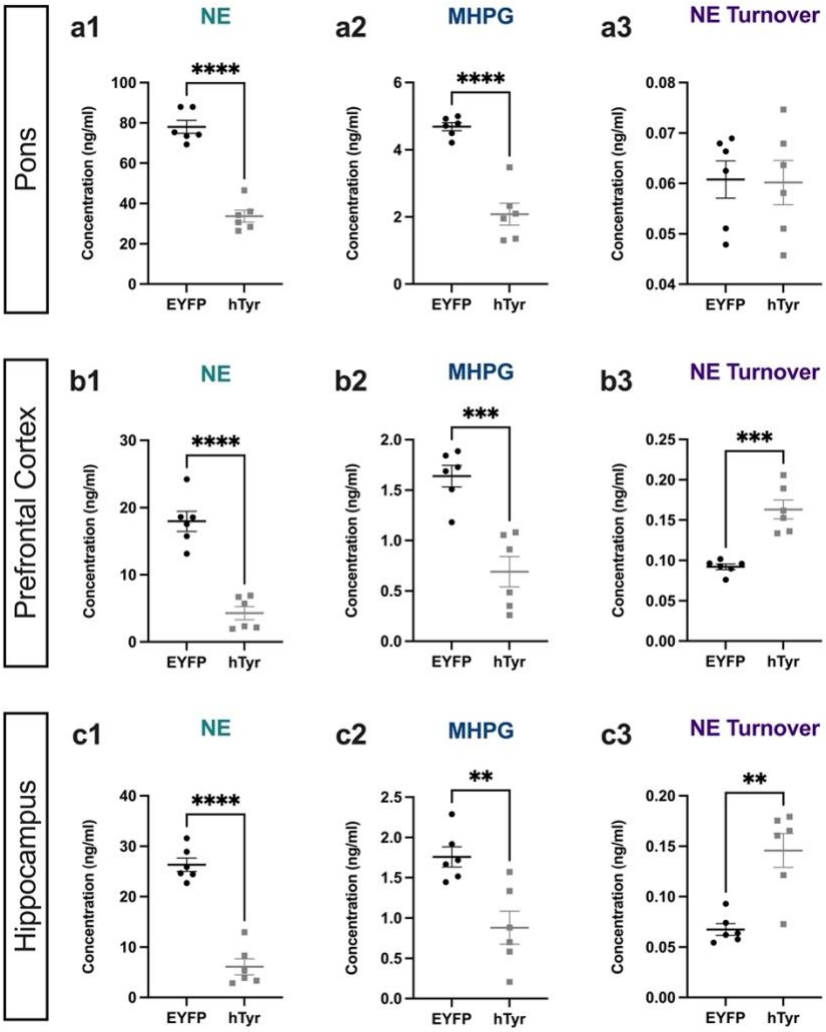

Fig. 3. hTyr-induced pigmentation decreases tissue NE and metabolite levels and increases turnover at 1 week. TH-Cre mice received stereotaxic infusion of AAV-DIO-hTyr or EYFP control into the LC, and tissue monoamine and metabolite levels were measured 1 week later by HPLC in the pons, prefrontal cortex (PFC), and hippocampus. hTyr significantly decreased NE and its primary metabolite MHPG in the pons (**a1-2**), PFC (**b1-2**), and hippocampus (**c1-2**). NE turnover, defined as the MHPG:NE ratio, was increased in PFC (**b3**) and hippocampus (**c3**). Data shown as mean ± SEM. N=6 per group. *p<0.05, **p<0.01, ****p<0.0001.

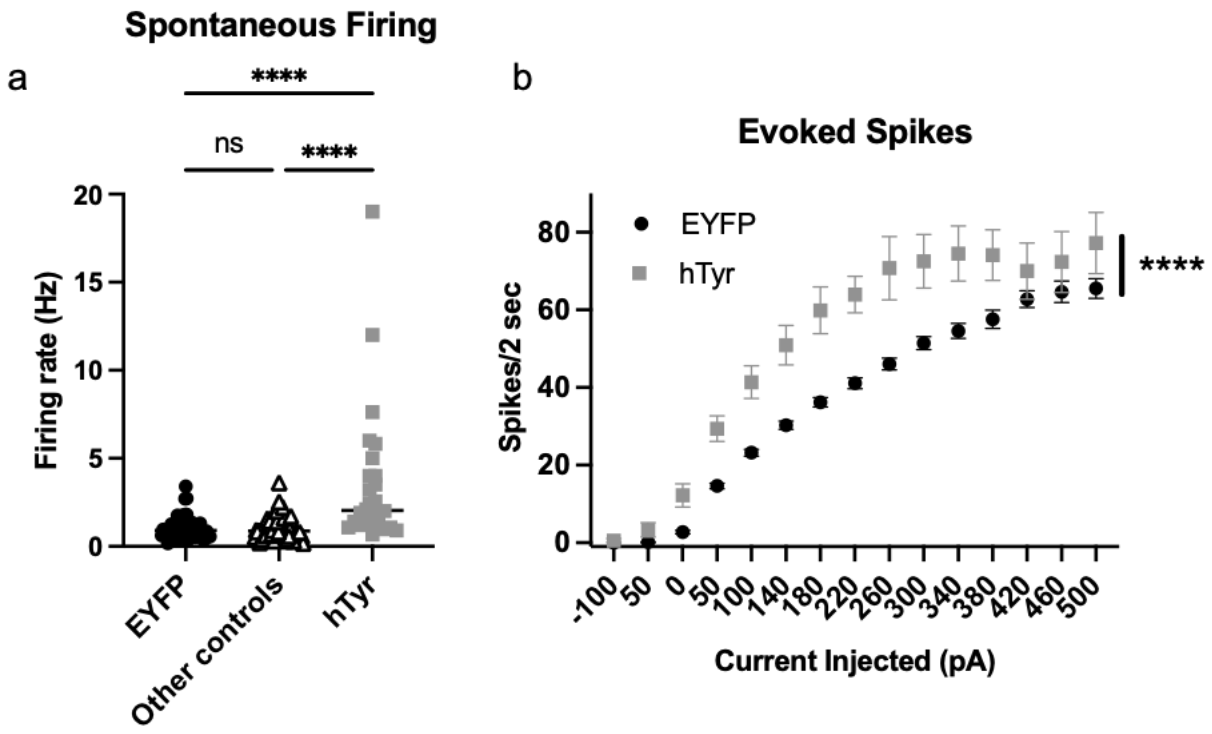

Fig. 4. hTyr-induced NM accumulation causes LC hyperactivity at 1 week. TH-Cre mice received stereotaxic infusion of AAV-DIO-hTyr or EYFP control into the LC, and LC neuron activity was assessed 1 week later by slice electrophysiology. (**a**) NM-containing LC neurons (N=26) had increased spontaneous firing compared to eYFP (N=55) or other controls (N=71; e.g. neighboring LC neurons in the hTyr group that were not expressing NM). (**b**) NM-containing LC neurons (N=24) fired more action potentials following current injection compared to EYFP LC neurons (N=77). ****p<0.0001.

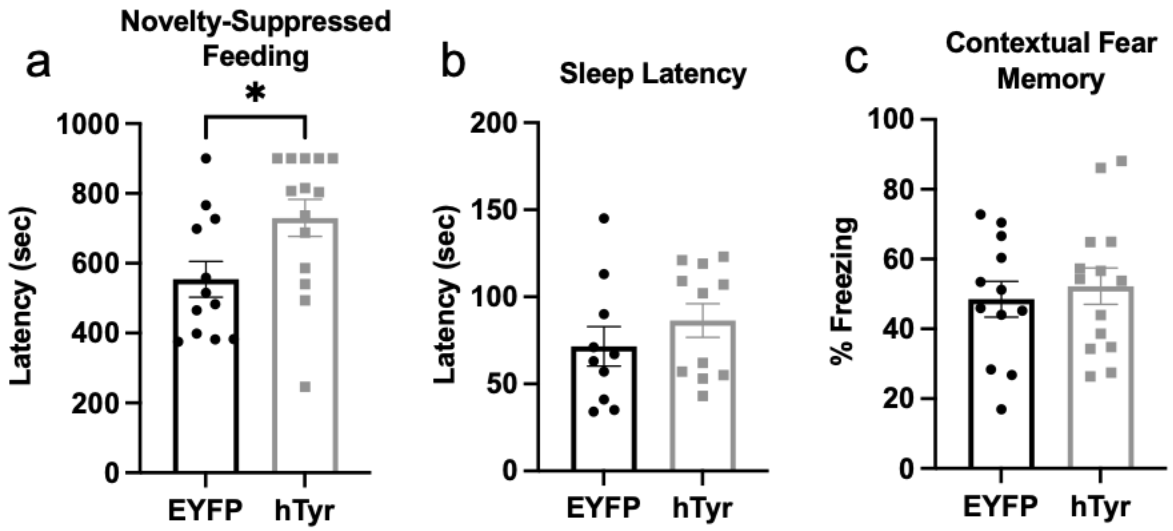

Fig. 5. hTyr-induced pigmentation increases anxiety-like behavior but not arousal or contextual fear memory at 1 week. TH-Cre mice received stereotaxic infusion of AAV-DIO-hTyr or EYFP control into the LC, and behavior was assessed 1 week later. hTyr-expressing mice displayed increased latency to bite the food pellet in the novelty-suppressed feeding test but no difference in latency to sleep in their home cage following gentle handling (**b**) or freezing behavior in the contextual conditioning fear assay (**c**). (N=12-14 per group). *p<0.05.

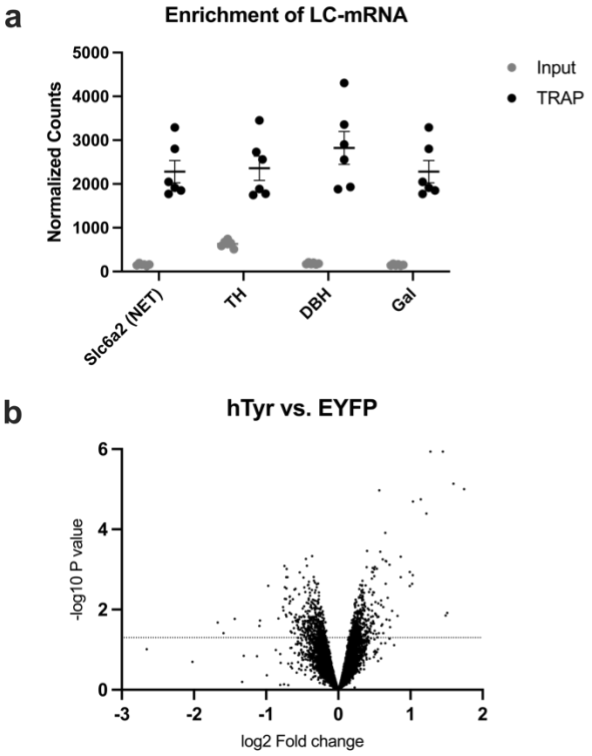

c

GeneSet	Pathway	Enrichment Score	p-value
KEGG	Tyrosine metabolism	0.62	0.008
KEGG	Tryptophan metabolism	0.60	0.014
KEGG	P53 signaling	0.51	0.018
KEGG	Adhesion molecules	0.41	0.030
KEGG	Melanoma	0.41	0.067
KEGG	Peroxisome	0.37	0.058
KEGG	Lysosome	0.35	0.042
KEGG	Calcium signaling	-0.43	0.010
KEGG	Oxidative phosphorylation	-0.41	0.032
KEGG	Alzheimer's disease	-0.37	0.075
HPO	Parkinsonism	0.54	0.039
HPO	Exaggerated startle response	0.56	0.047
HPO	Speech articulation	0.58	0.040
HPO	Sleep apnea	0.59	0.021
HPO	Delusions	-0.62	0.003
GO:BP	Regulation of extrinsic apoptotic signaling pathway	0.70	0.000
GO:BP	Antigen processing and presentation via MHC-I	0.74	0.000
GO:BP	Response to iron ion	0.61	0.018
GO:BP	Positive regulation of T-cell mediated immunity	0.61	0.027
GO:BP	Response to manganese ion	0.57	0.047
GO:BP	Dopamine metabolic process	0.49	0.047
GO:BP	Positive regulation of macroautophagy	0.47	0.011
GO:BP	Pigment metabolic process	0.46	0.024
GO:BP	Response to endoplasmic reticulum stress	0.42	0.00
GO:BP	Neuron death	0.30	0.011
GO:CC	Pigment granule	0.43	0.00

Fig. 6. hTyr-driven pigmentation triggers changes in the LC transcriptome. TH-Cre; Slc6a2-eGFP/Rpl10a mice received viral infusion of AAV5-DIO-hTyr or EYFP control in the LC, and gene expression was assessed 1 week later. We confirmed LC-mRNA enrichment in TRAP samples over hindbrain input, and found elevated levels of noradrenergic genes in the immunoprecipitated TRAP samples (**a**). Volcano plot of all filtered, normalized genes (~11,500) displaying spread of up- and down-regulated genes (**b**). Table highlighting significantly enriched KEGG, Human Phenotype Ontology (HPO), Gene Ontology Biological Process (GO:BP) and Gene Ontology Cellular Component (GO:CC) pathways of interest in our LC data (**c**).

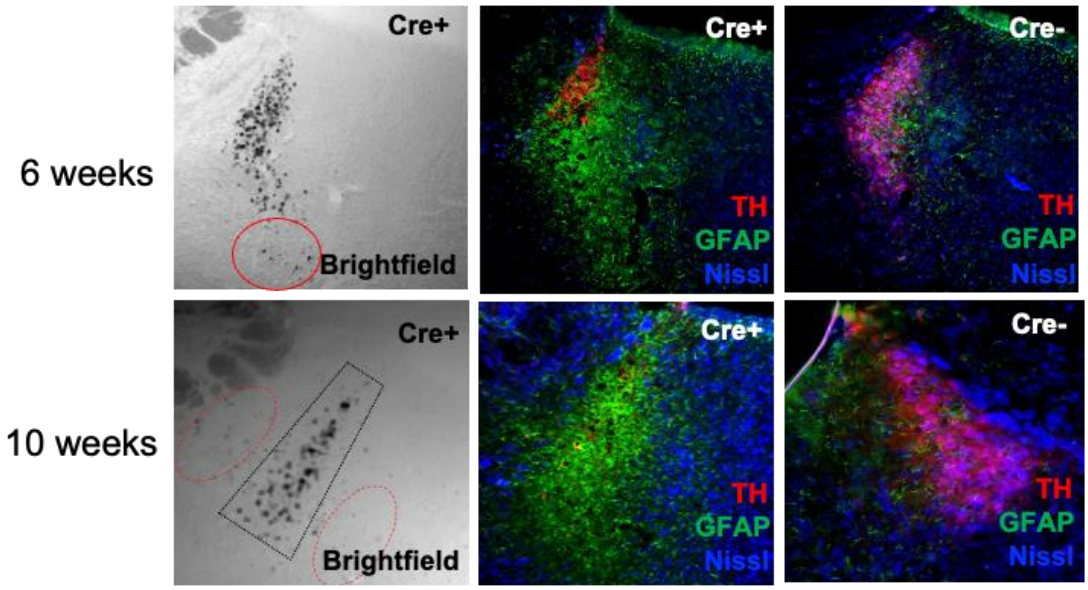

Fig. 7. Prolonged pigment expression results in granule accumulation and LC degeneration. TH-Cre+ and TH-Cre- mice received stereotaxic infusion of AAV-DIO-hTyr into the LC and aged for 6-10 weeks. Shown are representative images of NM (brightfield), the neuron marker Neurotrace Nissl (blue), the LC marker TH (red), and the astrocyte marker GFAP. Red ovals depict pigment outside the typical confines of the LC. Images were acquired at 20X magnification.

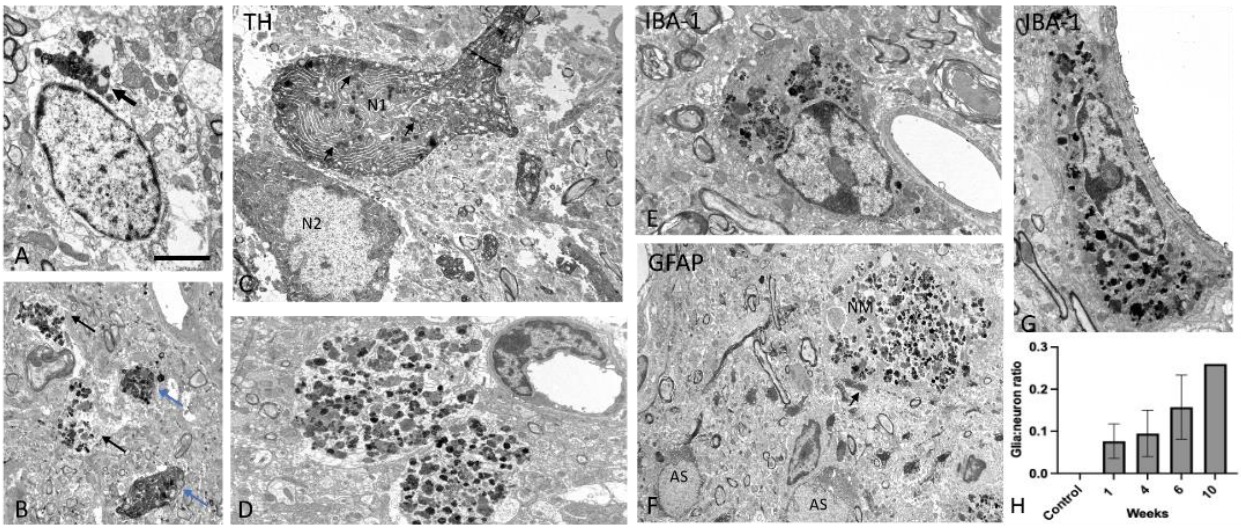

Fig. 8. Ultrastructual analysis of NM granules in the mouse LC. (**A**) Cluster of NM in the cell body of a LC neuron (arrow), (**B-C**) LC tissue immunostained for TH showing NM expression in TH-positive dendritic profiles (blue arrows in **B**) and a neuronal cell body (N1 in **C**). In B, the black arrows indicate NM-containing TH-negative dendrites, while in **C**, they point at intracellular NM granules. Note in **C**, a TH-positive LC neuronal perikaryon (N2) that does not contain NM. (**D**) Large neuropil structures heavily packed with NM granules. (**E,G**) Examples of IBA-1-positive microglia cell bodies enriched in NM aggregates. (**F**) GFAP-positive astrocytic profiles (AS) in the close vicinity of a NM-containing neuropil element. Note the lack of NM in AS cell bodies, and the close apposition between an AS process and the NM-containing element (arrow in **F**). (**H**) The ratio of NM-containing glia:neuron profiles in the LC of control (no hTyr; N=3) and experimental (hTyr 1 week, N=3; 4 weeks, N=2; 6 weeks N=4; 10 weeks N=1) mice. Scale bar value: A: 5 mm; B,C,F: 2 mm; D,E,G: 3 mm.

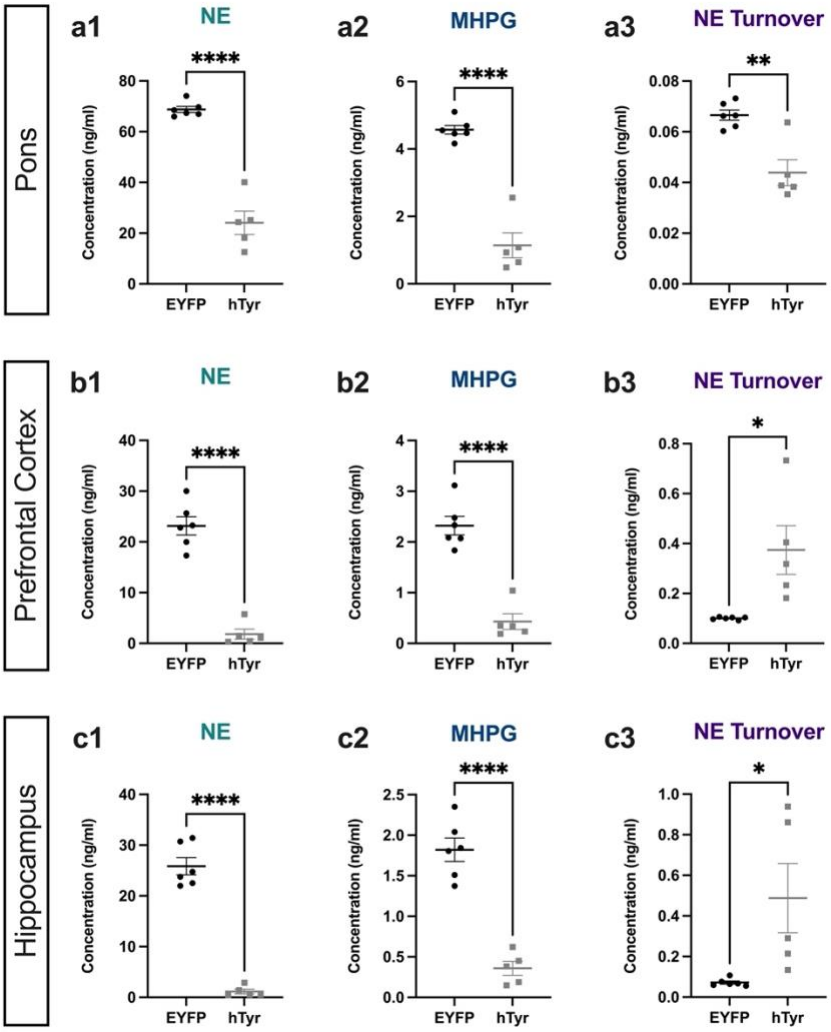

Fig. 9. hTyr-induced pigmentation depletes tissue NE and metabolite levels and dysregulates turnover at 6 weeks. TH-Cre mice received stereotaxic infusion of AAV5-DIO-hTyr or EYFP control into the LC, and tissue monoamine and metabolite levels were measured 6 weeks later by HPLC in the pons, prefrontal cortex (PFC), and hippocampus. hTyr significantly and robustly decreased NE and metabolite MHPG in the pons (**a1-2**), PFC (**b1-2**), and hippocampus (**c1-2**). NE turnover (MHPG:NE ratio) was decreased in the pons (**a3**), but decreased in the PFC (**b3**) and hippocampus (**c3**). Data shown as mean ± SEM. N=8 per group. *p<0.05, **p<0.01, ****p<0.0001.

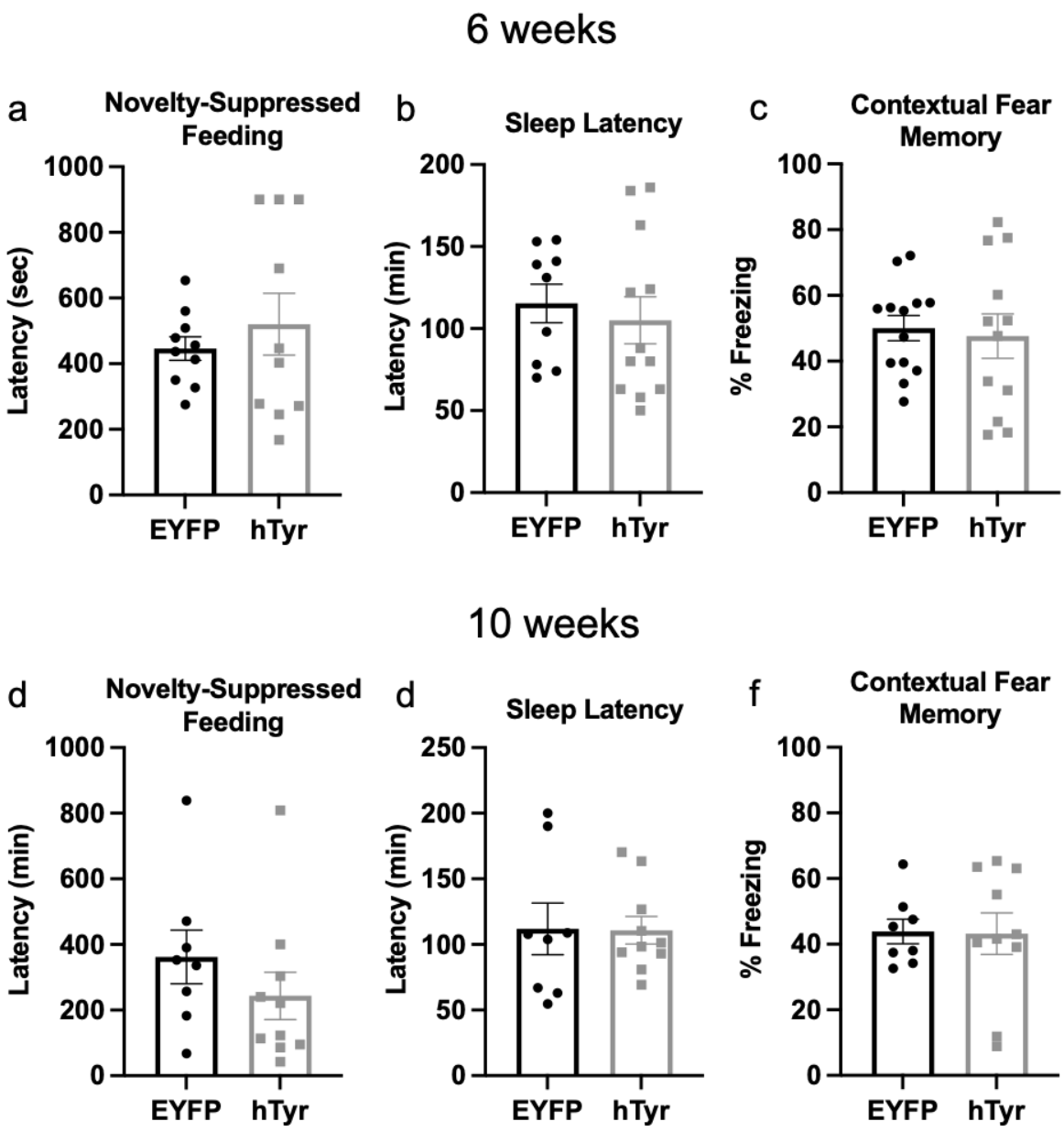

Fig. 10. Pigment accumulation and subsequent neurodegeneration has no effect on behavior. TH-Cre mice received stereotaxic infusion of AAV5-DIO-hTyr or EYFP control into the LC, and behavior was assessed 6 (**a-c**) or 10 weeks (**d-f**) later. hTyr-expressing mice displayed no difference in latency to eat in the novelty-suppressed feeding test (**a,d**), sleep latency (**b,e**), or freezing in response to shock-associated context (**c,f**) at either time point. (N=8-13 per group).

Table 1. IHC antibodies

Antibodies	Host	Manufacturer	Catalog #	Dilution
Tyrosine hydroxylase	Chicken	Abcam	ab76442	1:1000
Norepinephrine transporter	Mouse	Mab Technologies	NET05-2	1:1000
Human tyrosinase	Mouse	Thermo Fisher Scientific	MS-800-B1	1:500
GFAP	Guinea Pig	Synaptic Systems	173 004	1:1000
NeuroTrace 435/455 Blue Fluorescent Nissl Stain	NA	Thermo Fisher Scientific	N21479	1:500
Alexa Fluor 488 Anti-Rabbit	Goat	Thermo Fisher Scientific	A-11008	1:500
Alexa Fluor 488 Anti-Guinea Pig	Goat	Thermo Fisher Scientific	A-11073	1:500
Alexa Fluor 568 Anti-Chicken	Goat	Thermo Fisher Scientific	A-11041	1:500

Table 2. Monoamine levels measured by HPLC. Data shown as mean ± SEM. N=5-6 per group.

A) 1-week post-infusion

	Pons		PFC		Hippocampus	
	EYFP	**hTyr**	**EYFP**	**hTyr**	**EYFP**	**hTyr**
DA	11.37 ± 0.69	10.39 ± 0.91	20.14 ± 8.32	4.54 ± 0.38	3.53 ± 1.29	2.33 ± 0.28
DOPAC	6.98 ± 0.49	7.53 ± 0.72	3.08 ± 0.61	2.40 ± 0.20	2.52 ± 0.26	2.47 ± 0.45
DOPAC:DA	0.62 ± 0.03	0.72 ± 0.02	0.30 ± 0.08	0.53 ± 0.02	1.04 ± 0.20	1.11 ± 0.19
5-HT	170.9 ± 3.38	162.5 ± 4.33	40.66 ± 3.34	45.30 ± 2.94	69.17 ± 3.43	63.04 ± 3.73
5-HIAA	58.31 ± 3.09	61.95 ± 4.11	7.72 ± 0.22	8.59 ± 0.45	7.72 ± 0.22	8.59 ± 0.45
5-HIAA:5-HT	0.34 ± 0.02	0.38 ± 0.20	0.20 ± 0.02	0.19 ± 0.01	0.36 ± 0.03	0.38 ± 0.01

B) 6-weeks post-infusion

	Pons		PFC		Hippocampus	
	EYFP	**hTyr**	**EYFP**	**hTyr**	**EYFP**	**hTyr**
DA	9.14 ± 0.90	7.33 ± 1.06	43.34 ± 22.50	30.36 ± 16.71	2.54 ± 0.61	1.99 ± 0.37
DOPAC	6.34 ± 0.49	5.39 ± 0.70	6.33 ± 1.99	5.22 ± 1.31	1.75 ± 0.18	2.74 ± 0.28
DOPAC:DA	0.71 ± 0.05	0.75 ± 0.08	0.30 ± 0.06	0.28 ± 0.07	0.84 ± 0.16	1.53 ± 0.22
5-HT	162.6 ± 6.20	146.7 ± 4.90	62.40 ± 5.61	57.03 ± 3.27	71.83 ± 3.84	71.54 ± 3.64
5-HIAA	71.80 ± 5.58	50.41 ± 1.68	13.65 ± 2.19	10.02 ± 0.27	31.89 ± 2.02	23.78 ± 0.78
5-HIAA:5-HT	0.44 ± 0.02	0.35 ± 0.02	0.21 ± 0.01	0.18 ± 0.01	0.45 ± 0.02	0.34 ± 0.03